Vinculin targeting by *Shigella* IpaA promotes stable cell adhesion independent of mechanotransduction

Cesar Valencia-Gallardo[1-4]*, Daniel-Isui Aguilar-Salvador[1-4]*, Hamed Khakzad[5, 7§], Charles Bou-Nader[8, 9§], Christian Malosse[10], Diogo Borges Lima[10], Chakir Bello[1-4], Benjamin Cocom-Chan[1-4], Nicole Quenech'Du[1-4], Bilal Mazhar[1-4], Delphine Javelaud[11-13], Jacques Fattaccioli[14, 15], Alain Mauviel[11-13], Marc Fontecave[8, 9], Atef Asnacios[16], Julia Chamot-Rooke[10], Lars Malmström[5, 7, 17], Guy Tran Van Nhieu[1-4¶*]

[1]Equipe Communication Intercellulaire et Infections Microbiennes, Centre de Recherche Interdisciplinaire en Biologie (CIRB), Collège de France, 75005 Paris, France

[2]Institut National de la Santé et de la Recherche Médicale U1050, 75005 Paris, France

[3]Centre National de la Recherche Scientifique UMR7241, 75005 Paris, France

[4]MEMOLIFE Laboratory of excellence and Paris Science Lettre

[5]Institute for Computational Science, University of Zürich, Zürich, Switzerland.

[6]S3IT, University of Zürich, Zürich, Switzerland.

[7]Swiss Institute of Bioinformatics, Lausanne, Switzerland.

[8]Laboratoire de Chimie des Processus Biologiques, Collège De France, 75005 Paris, France.

[9]Centre National de la Recherche Scientifique UMR8229, 75005 Paris, France

[10] Mass Spectrometry for Biology Utechs, Institut Pasteur, USR 2000, CNRS, 75015 Paris, France

[11]Institut Curie, PSL Research University, INSERM U1021, CNRS UMR3347, Team "TGF-ß and Oncogenesis", Equipe Labellisée LIGUE 2016, F-91400, Orsay, France.

[12]Université Paris-Sud, F-91400, Orsay, France.

22 [13]Centre National de la Recherche Scientifique UMR 3347, 91400 Orsay, France

23 [14]PASTEUR, Département de Chimie, École Normale Supérieure, PSL University, Sorbonne Université,
24 CNRS, 75005 Paris, France

25 [15]Institut Pierre-Gilles de Gennes pour la Microfluidique, 75005 Paris, France

26 [16]Laboratoire Matière et Systèmes Complexes, UMR 7057 CNRS & Université Paris Diderot, Sorbonne
27 Paris Cité, Paris, France

28 [17]Division of Infection Medicine, Department of Clinical Sciences, Lund University, Lund, Sweden.

29 *, §equal contribution

30 ¶For correspondence:

31 E-mail: guy.tran-van-nhieu@college-de-france.fr. Tel: 33-1-44-27-14-89. FAX: 33-1-44-27-14-19

32 ***Shigella*, the causative agent of bacillary dysentery, invades epithelial cells by injecting type**
33 **III effectors that locally reorganize the actin cytoskeleton[1]. The type III effector IpaA targets the**
34 **focal adhesion protein vinculin to induce bacterial adhesion associated with the recruitment of**
35 **mature focal adhesion markers, despite the inability of bacteria to exert significant counter-forces[2,**
36 **[3]. Here, we show that three vinculin-binding sites (VBSs) exposed at the IpaA C-terminus act in a**
37 **cooperative manner to trigger a yet unreported mode of vinculin activation through specific**
38 **interactions with sites in the vinculin head sub-domain D2. Structural modeling based on the mass**
39 **spectrometry identification of interacting residues by cross-linking indicated that upon IpaA**
40 **binding to vinculin D2, vinculin head sub-domains undergo major conformational changes leading**
41 **to higher order heterocomplexes and vinculin homo-trimers. IpaA-mediated vinculin activation**
42 **induces the formation of large and stable focal adhesions resisting the action of actin relaxing**
43 **drugs. This property enables IpaA to rapidly elicit strong cell adhesion to fibronectin-coated**
44 **substrates. While *Shigella* IpaA promotes strong adhesion in the absence of mechanotransduction,**

45 **its mode of vinculin activation likely reflects a key step during maturation of cell adhesions driven**
46 **by acto-myosin contractility.**

47 Integrin-mediated cell adhesion critically depends on the cytoskeletal linkers talin and
48 vinculin[4-6]. During mechanotransduction, talin acts as a mechanosensor by exposing its VBSs as a
49 function of the stretching force generated by acto-myosin and dependent on substrate stiffness[7].
50 Talin exposed VBSs recruit and activate vinculin, reinforcing anchorage to the actin cytoskeleton in
51 response to mechanical load[8, 9]. Vinculin contains three repetitions (D1-D3) of a conserved domain
52 consisting of two bundles of four helices, and a fourth D4 domain containing only one helical bundle
53 connected to a proline-rich unstructured region and the carboxyterminal F-actin binding domain[10].
54 Under its inactive folded form, intramolecular interactions between the vinculin head and tail
55 domains prevent ligand binding.

56 The *Shigella* type III invasion effector IpaA contains 3 VBSs located in its carboxyterminal
57 moiety[11-13]. IpaA VBS1, as for all VBSs described to date to promote vinculin activation, interacts with
58 the first helical bundle of the D1 domain, promoting major conformational changes that disrupt the
59 D1-tail intramolecular interactions and free the vinculin F-actin binding region[11] (Fig. 1a). IpaA VBS2,
60 in contrast, interacts with the second helical bundle of D1[12] (Fig. 1a) and its association with IpaA
61 VBS1 results in a very high affinity and stable IpaA VBS1-2:D1 complex ,with an estimated K_D in the
62 femtoM range[12]. While functional evidence indicates that IpaA VBS3 cooperates with IpaA VBS1-2 to
63 stimulate bacterial invasion, the isolated peptide acts as IpaA VBS1 in promoting vinculin activation
64 through interaction with the vinculin D1 first helical bundle and also forms a folded bundle with the
65 talin H1-H4 helices[13, 14].

66 Here, we studied the effects of the IpaA subdomains containing VBS1-2 (A524) or VBS1-3
67 (A483) on vinculin activation (Fig. 1b). We performed SEC-MALS (Size Exclusion Chromatography-
68 Multi-Angle Light Scattering) to analyze complexes formed upon incubation of A483 with HV_{1-834}
69 containing the D1-D4 domains, corresponding to full-length human vinculin (HV) devoid of the

70 carboxyterminal F-actin binding domain (Fig. 1b). In addition to the 1:1 D1D4: A483 complex, larger
71 complexes were observed corresponding to a 2:1 heterocomplex and a 3:0 D1-D4 homo-trimer (Fig.
72 1c). Similar 2:1 and 3:0 complexes were observed when A483 was incubated with HV_{1-484} containing
73 only the vinculin D1 and D2 domains (D1D2) (Fig. 1d), indicating that vinculin homo-trimerization
74 occurs exclusively through these vinculin head sub-domains. By contrast, when A524 was incubated
75 with D1D2, 1:1 and 2:1 D1D2:A524 complexes were detected, but not the D1D2 homo-trimer
76 suggesting a role for IpaA VBS3 in vinculin trimerization (Fig. 1d). Consistently, higher order D1D2
77 homo-complexes devoid of A483 and D1D2:A524 hetero-complexes were visualized by native PAGE
78 (Fig. 1e and Suppl. Figs. 3c, d). These results suggest that binding of IpaA VBSs to vinculin triggers
79 conformational changes in vinculin leading to the formation of an IpaA VBS3-dependent vinculin
80 homo-trimer.

81 To further investigate initial interactions responsible for vinculin trimer formation, w e performed
82 binding assays with HV derivatives immobilized onto a solid phase to restrict conformational changes.
83 These assays indicated that A483 and A524 bound to HV with a similar affinity, as estimated by their
84 EC50 (95% confidence interval) of 6.1 (4.2-9.0) and 3.7 (1.7-8.1) nM, respectively (Suppl. Fig. 1a).
85 Strikingly, a large difference was observed in the binding plateau, indicating that HV presented more
86 binding sites for A483 than for A524 (Suppl. Fig. 1a). Also, D1D2 presented more binding sites for
87 HV_{1-258} containing the D1 domain only, suggesting the presence of additional sites on the D2 domain
88 (Suppl. Fig. 1b). Consistently, BN-PAGE showed the formation of 1:1, as well as a 1:2 D1D2:A483
89 complex, observed with increasing A483 molar ratio (Suppl. Fig. 1c). In contrast, single 1:1 complexes
90 were observed for D1:A483, D1:A524 or D1D2-A524 (Suppl. Figs. 1c-h), indicating that IpaA VBS3 was
91 required to reveal additional sites on the D2 domain. Of note, D1D2 homo-trimers observed in the
92 SEC-MALS and native gel analysis (Figs. 1d, e and Ext Data Figs. 3c, d) were not detected in BN-PAGE,
93 suggesting that Coomassie brilliant blue interfered with the formation of higher order D1D2
94 complexes. Together, these results suggested that the formation of vinculin trimers triggered by
95 A483 required the IpaA VBS3 dependent exposure of binding sites on D2. These findings were

96 unexpected, since vinculin activating ligands have been described to bind to a single site on the D1
97 domain of vinculin.

98 To map interactions of A524 and A483 with D1D2, complexes were cross-linked, subjected to
99 proteolysis and analyzed using Liquid Chromatography coupled to Mass Spectrometry (LC-MS)
100 (Methods). Intermolecular links were identified from the characterization of cross-linked peptides
101 (Suppl. Tables 1-3; Methods) and along with identified intramolecular links, used to produce
102 structural models (Methods). The A524:D1 complex showed links consistent with a "canonical"
103 conformer expected from established structures[11, 12, 15] (Suppl. Fig. 2). Similar links were identified for
104 the A524:D1D2 complex, with a majority of links observed with the D1 domain (Fig. 2a). For both
105 complexes, the structure shows interactions between IpaA VBS1 and VBS2 with the D1 first and
106 second bundles, respectively, leading to helical bundle reorganization of D1 associated with vinculin
107 activation (Figs. 2c, d; Suppl. Fig. 2 and Suppl. Tables 1, 2). For the A483:D1D2 complex, structural
108 modeling shows 2 major conformers accounting for the majority of links. In a first "closed"
109 conformer, IpaA VBS1 and VBS2 interact with the D1 bundles in a similar manner as for A524, where
110 the relative positioning of D1 and D2 is globally conserved compared to apo D1D2 in the A524-D1D2
111 complex (compare Figs. 2d and 2e). In this “closed” conformer, IpaA VBS3 interacts with an interface
112 formed by the H5 (residues 128-149) and H8 (residues 222-250) helices in the second bundle of D1
113 and the H13 (residues 373-397) helix in the second bundle of the D2 domain (Figs. 2e and f). The
114 second "open" conformer, however, shows a major re-orientation of D1 and D2 subdomains with
115 their major axis forming an angle value of ca 82° compared to the 25° observed in the native vinculin
116 structure or the first conformer (Fig. 2g), with IpaA VBS3 docking sidewise through extensive
117 interaction with the H5 (residues 128-149) and H8 (residues 222-250) helices of the vinculin D1
118 domain. Because this latter conformer leads to major changes in bundle exposure in D1 and D2, we
119 posit that it is involved in the formation of higher order D1D2 complexes and trimer induced by A483.
120 To test this, we engineered a structural clamp by substituting residue Q68 in the first D1 bundle and
121 A396 in the second D2 bundle for cysteine residues, expected to prevent the formation of the open

122 conformer upon disulfide bridge formation (Suppl. Figs. 3a, b). Consistently, cysteine clamped D1D2-
123 Q68C A396C did not prevent the exposure of additional sites on D2 or 1:1 complex formation induced
124 by A524 or A483, but prevented the formation of higher order complexes (Fig. 1 e and Suppl. Figs. 3c-
125 e). We coined "supra-activation" the mode of vinculin activation induced by A483 involving major
126 conformational changes in the vinculin head, to distinguish it from the canonical activation
127 associated with the dissociation of vinculin head-tail domains.

128 We then characterized the effects of A524 and A483 expression by performing
129 immunofluorescence staining of vinculin-containing adhesion structures. As shown in Figs 3a-c, C2.7
130 cells transfected with GFP-A524 formed more numerous and larger peripheral adhesions as well as
131 actin-rich ruffles compared to control cells (Figs. 3a-d). Strikingly, GFP-A483 transfected cells formed
132 even larger and more numerous adhesions than GFP-A524 transfected cells, but significantly less
133 actin ruffles than GFP-A524 transfectants (Figs. 3a-d). These observations were confirmed by live TIRF
134 microscopy showing the extreme stability of adhesions in GFP-A483 transfectants, with a median
135 duration of at least 84 min, while GFP-A524 and control cells showed adhesions with a comparable
136 median duration of less than 25 min (Fig. 3e; Suppl. movie 1). GFP-A524 and GFP-A483 transfectants
137 showed slightly slower median instant rates of adhesion assembly than control cells (Suppl. Fig. 4;
138 Suppl. movie 1) but significant 1.6-fold and 2-fold decrease in median instant rates of disassembly
139 relative to control cells, respectively (Suppl. Fig. 4). The stability of GFP-A483-induced FAs was
140 independent of acto-myosin contraction. Indeed, GFP-A483-induced FAs resisted the action of the
141 Rho-kinase inhibitor Y27632 relaxing actin-myosin, with a five- and four-times slower median rate of
142 disassembly of adhesions relative to control cells and GFP-A524 transfectants, respectively (Figs. 3f-i;
143 Suppl. movie 2). Furthermore, large adhesions formed in GFP-A483 transfectants following addition
144 of the inhibitor (Figs. 3f, h), a process that was not observed for the other samples, including cells
145 transfected with GFP-A524 or GFP fused to the vinculin D1 domain (vD1) reported to delay talin
146 refolding following stretching [16-18] (Figs. 3g-i; Suppl. movie 2). In line with the stabilization of mature
147 FAs through vinculin supra-activation, GFP-A483 but not GFP-vD1 also delayed the Y27632-induced

148 removal of the late adhesion marker VASP (Suppl. Fig. 5; Suppl. movie 3). Consistent with A483
149 bypassing mechanotransduction, GFP-A483 expression induced 5- and 1.6-fold higher yield of short
150 term (≤ 10 min) cell adhesion to fibronectin substrates compared to control GFP and GFP-A524
151 transfectants, respectively (Suppl. Fig. 6a). By contrast, little difference in adhesion yield was
152 detected at 15 min suggesting that canonical activation of vinculin also resulted in its supra-activation
153 during mechanotranduction (Suppl. Fig. 6a). In line with this, MEF vinculin-null cells transfected with
154 the clamped vinculin version formed fewer and smaller FAs than cells transfected with wild-type
155 vinculin but more than mock-transfected cells (Suppl. Figs. 6b-d).

156 To confirm and extend these findings, cell adhesion strength was assessed measuring their
157 detachment upon application of a controlled shear stress in a microfluidic chamber. When 1205Lu
158 melanoma cells were allowed to adhere to fibronectin-coated surfaces for more than 25 min, little
159 difference in resistance to shear stress could be detected among samples (Suppl. Fig. 7a). In contrast,
160 when shear stress was applied less than 20 min following cell incubation, GFP-A483-transfected cells
161 showed significantly higher resistance to shear stress up to 22.2 dynes.cm^{-2} than GFP-A524- or GFP-
162 transfected cells, with 1.7 ± 0.2 -and 0.9 ± 0.14-fold enrichment ± SD of adherent cells for GFP-A483
163 and GFP-A524-transfected cells versus control GFP-transfected cells, respectively (Fig. 4b; Suppl.
164 movie 4). In addition, similar to melanoma cells depleted for by siRNA treatment, cells transfected
165 with the clamped vinculin version showed a decreased ability to adhere in comparison to WT
166 vinculin-transfected cells (Suppl. Figs. 7a, b). These results are in full agreement with effects observed
167 on adhesion structures and suggest that A483 interaction with vinculin leads to the bypass of
168 mechanotransducing steps to promote strong adhesion.

169 Vinculin is paradoxically described as a prognostic marker favoring the migration of cancer cells
170 or as a tumor suppressor stimulating cell anchorage [19-21]. These contradictory findings reflect its
171 complex and poorly understood regulation, as well as different roles in 2D or 3D systems [22, 23]. Also,
172 an increase of the total pool of vinculin may not correlate with increased vinculin activation. We took
173 advantage of the unique property of A483 to study the effects of vinculin supra-activation on the

174 motility and invasion of melanoma cells. In time-lapse microscopy experiments in 2D-chambers, GFP-
175 A524 inhibited melanocyte motility compared to control cells, with a rate of Root Median Square
176 Displacement (rMSD) of 3.16 and 15.6 µm.min, respectively (Figs. 4c, d). An even stronger inhibition
177 was observed for GFP-A483-transfected cells (rMSD = 2.3 µm.min) (Figs. 4c, d). Transmigration of
178 melanocytes in 3D-matrigels was similarly inhibited by A524 and A483 (Fig. 4e).

179 Bacteria invading through a triggering mode rely on a discrete number of T3SS-dependent
180 contacts for which cytoskeletal tethering is likely critical for invasion[2]. As opposed to physiological
181 substrates, bacteria cannot sustain the range of counter-forces associated with integrin-mediated
182 adhesion to the substrate. The *Shigella* type III effector IpaA provides an elegant solution to this
183 problem by promoting strong adhesion without requirement for mechanotransduction. Through the
184 joint action of its VBSs, IpaA induces major conformational changes of the vinculin head sub-
185 domains. Understanding how these major vinculin conformational changes regulate the composition
186 and properties of cell adhesions will bring important insights into cell adhesion processes and will be
187 the focus of future investigations.

188 **REFERENCES**

189 1 Ogawa, M., Handa, Y., Ashida, H., Suzuki, M. & Sasakawa, C. The versatility of *Shigella* effectors.
190 *Nat Rev Microbiol* **6**, 11-16, doi:10.1038/nrmicro1814 (2008).
191 2 Valencia-Gallardo, C. M., Carayol, N. & Tran Van Nhieu, G. Cytoskeletal mechanics during *Shigella*
192 invasion and dissemination in epithelial cells. *Cellular microbiology* **17**, 174-182,
193 doi:10.1111/cmi.12400 (2015).
194 3 Tran Van Nhieu, G., Ben-Ze'ev, A. & Sansonetti, P. J. Modulation of bacterial entry into epithelial
195 cells by association between vinculin and the *Shigella* IpaA invasin. *The EMBO journal* **16**, 2717-
196 2729, doi:10.1093/emboj/16.10.2717 (1997).
197 4 Atherton, P., Stutchbury, B., Jethwa, D. & Ballestrem, C. Mechanosensitive components of
198 integrin adhesions: Role of vinculin. *Exp Cell Res*, doi:10.1016/j.yexcr.2015.11.017 (2015).

199 5 Yan, J., Yao, M., Goult, B. T. & Sheetz, M. P. Talin Dependent Mechanosensitivity of Cell Focal
200 Adhesions. *Cellular and molecular bioengineering* **8**, 151-159, doi:10.1007/s12195-014-0364-5
201 (2015).
202 6 Burridge, K. & Guilluy, C. Focal adhesions, stress fibers and mechanical tension. *Exp Cell Res*,
203 doi:10.1016/j.yexcr.2015.10.029 (2015).
204 7 Parsons, J. T., Horwitz, A. R. & Schwartz, M. A. Cell adhesion: integrating cytoskeletal dynamics
205 and cellular tension. *Nat Rev Mol Cell Biol* **11**, 633-643, doi:10.1038/nrm2957 (2010).
206 8 Humphries, J. D. *et al.* Vinculin controls focal adhesion formation by direct interactions with talin
207 and actin. *J Cell Biol* **179**, 1043-1057, doi:10.1083/jcb.200703036 (2007).
208 9 Lavelin, I., Wolfenson, H., Patla, I., Henis, Y. I., Medalia, O., Volberg, T., Livne, A., Kam, Z., Geiger,
209 B**.** Differential effect of actomyosin relaxation on the dynamic properties of focal adhesion
210 proteins. PLoS One. 8:e73549 (2013).
211 10 Bakolitsa, C. *et al.* Structural basis for vinculin activation at sites of cell adhesion. *Nature* **430**,
212 583-586, doi:10.1038/nature02610 (2004).
213 11 Izard, T., Tran Van Nhieu, G. & Bois, P. R. Shigella applies molecular mimicry to subvert vinculin
214 and invade host cells. *J Cell Biol* **175**, 465-475, doi:10.1083/jcb.200605091 (2006).
215 12 Tran Van Nhieu, G. & Izard, T. Vinculin binding in its closed conformation by a helix addition
216 mechanism. *The EMBO journal* **26**, 4588-4596, doi:10.1038/sj.emboj.7601863 (2007).
217 13 Park, H., Valencia-Gallardo, C., Sharff, A., Tran Van Nhieu, G. & Izard, T. Novel vinculin binding
218 site of the IpaA invasin of *Shigella*. *J Biol Chem* **286**, 23214-23221, doi:10.1074/jbc.M110.184283
219 (2011).
220 14 Valencia-Gallardo C, Bou-Nader C, Aguilar D, Carayol N, Quenech'Du N, Pecqueur L, Park HJ,
221 Fontecave M, Izard T, Tran Van Nhieu G. *Shigella* IpaA binding to talin stimulates filopodial
222 capture and cell adhesion. *Cell Reports* **26**, 921-932. doi: 10.1016/j.celrep.2018.12.091 (2019).
223 15 Izard, T. *et al.* Vinculin activation by talin through helical bundle conversion. *Nature* **427**, 171-
224 175, doi:10.1038/nature02281 (2004).

225 16 del Rio, A. *et al.* Stretching single talin rod molecules activates vinculin binding. *Science* **323**, 638-
226 641, doi:10.1126/science.1162912 (2009).
227 17 Margadant, F. *et al.* Mechanotransduction in vivo by repeated talin stretch-relaxation events
228 depends upon vinculin. *PLoS Biol* **9**, e1001223, doi:10.1371/journal.pbio.1001223 (2011).
229 18 Carisey, A. *et al.* Vinculin regulates the recruitment and release of core focal adhesion proteins in
230 a force-dependent manner. *Curr Biol* **23**, 271-281, doi:10.1016/j.cub.2013.01.009 (2013).
231 19 Goldmann, W. H. Role of vinculin in cellular mechanotransduction. *Cell Biol Int* **40**, 241-256,
232 doi:10.1002/cbin.10563 (2016).
233 20 Labernadie, A. *et al.* A mechanically active heterotypic E-cadherin/N-cadherin adhesion enables
234 fibroblasts to drive cancer cell invasion. *Nat Cell Biol* **19**, 224-237, doi:10.1038/ncb3478 (2017).
235 21 Hamidi, H. & Ivaska, J. Every step of the way: integrins in cancer progression and metastasis. *Nat*
236 *Rev Cancer*, doi:10.1038/s41568-018-0038-z (2018).
237 22 Mierke, C. T. *et al.* Vinculin facilitates cell invasion into three-dimensional collagen matrices. *J*
238 *Biol Chem* **285**, 13121-13130, doi:10.1074/jbc.M109.087171 (2010).
239 23 Gulvady, A. C., Dubois, F., Deakin, N. O., Goreczny, G. J. & Turner, C. E. Hic-5 expression is a
240 major indicator of cancer cell morphology, migration, and plasticity in three-dimensional
241 matrices. *Mol Biol Cell* **29**, 1704-1717, doi:10.1091/mbc.E18-02-0092 (2018).
242

243 **ACKNOWLEDGEMENTS**

244 The authors thank Gauthier Mercante for technical help, Philippe Mailly for help with image
245 analysis and René-Marc Mège for insightful discussions and reading of the manuscript. This work was
246 supported by grants from Inserm, CNRS and Collège de France to the CIRB, as well as grant from the
247 PSL Idex project "Shigaforce". DIAS and BCC are recipients of a PhD fellowship from a CONACYT
248 scholarship. CV-G and DIAS also received support from the Memolife Labex. HK and LM were
249 supported by Swiss National Science Foundation (grant no. SNF 200021 160188) and LM by the Knut
250 And Alice Wallenberg Foundation (grant no. KAW 2016.0023).

251 **AUTHOR CONTRIBUTIONS**

252 CV-G and DIAS conceived and performed most of the experimental works, data analysis and
253 wrote the manuscript. BCC and BM analyzed TIRF experiments. CB-N performed the SEC-MALS
254 analysis. CB and NQD performed and analyzed experiments with melanocytes with the help of DJ and
255 AM. BCC, AA and JF provided technical help for cell adhesion and microfluidics experiments. CM and
256 JCR designed and performed the LC-MS analysis. DBL analyzed the cross-linked mass spectrometry
257 data. HK and LM generated structural models. GTVN designed the project and wrote the manuscript.

258

259 **FIGURES AND LEGENDS**

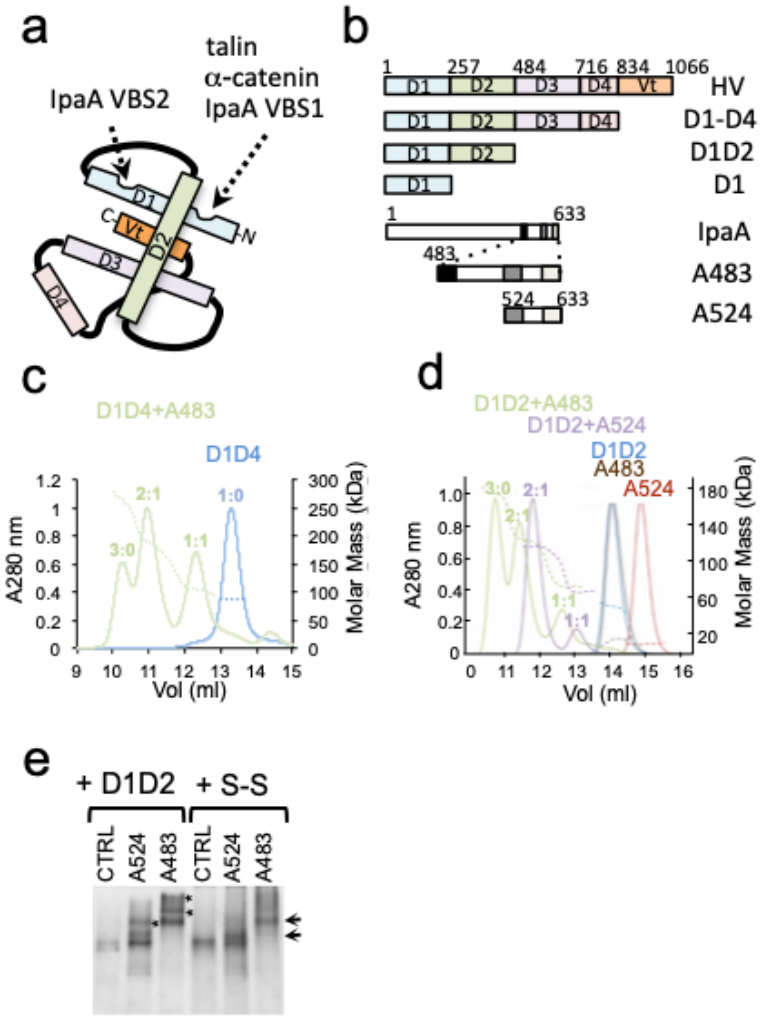

260

261 **Figure 1 – IpaA reveals binding sites in vinculin head subdomains**

262 **a,** Scheme of folded vinculin (HV). The binding sites and corresponding ligands are indicated. **b,**
263 Scheme of HV and IpaA constructs. HV domains and IpaA VBSs are depicted as boxes. The numbers
264 indicate the start residue of each domain. **c, d,** SEC elution profiles of complexes formed between A483
265 (green) or A524 (purple) and vinculin D1D4 (**c**) or D1D2 (**d**). The indicated complex stoichiometry was
266 inferred from the molecular weight estimated by MALS. **e**, native gel analysis of vinculin D1D2 and IpaA
267 derivatives. D1D2 or cysteine-clamped D1D2 (S-S) were incubated with the indicated IpaA derivatives
268 and analyzed by native PAGE followed by Coomassie staining. Arrows: 1:1 complexes. *: higher order
269 complexes. Note the absence of higher order complexes for cysteine-clamped D1D2.

270

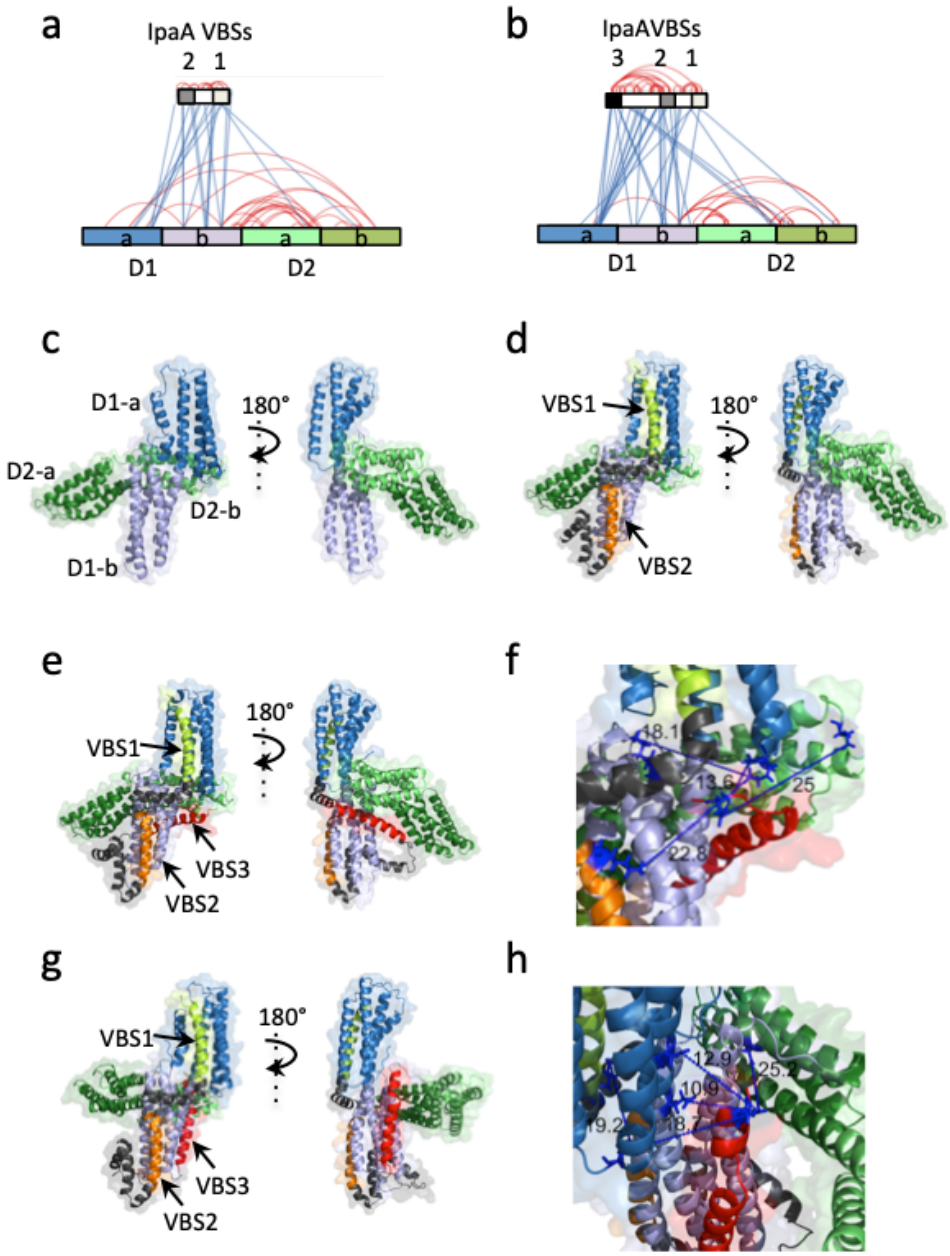

271

272 **Figure 2 – Characterization of IpaA contact sites on vinculin.**

273 **a**, **b**, EDC cross-link map from mass spectrometry analysis (LC-MS/MS) of vinculin D1D2-A524 (**a**) and

274 D1D2-A483 (**b**) following extraction of 1:1 complexes from BN-PAGE. Blue lines: inter-molecular links.

275 Red lines: intra-molecular links. Note the links between IpaA VBS3 and the D2 second bundle. Cross-

276 linked residues are detailed in Suppl. Table 1. **c-e**) Structural models of D1D2 (**c**), D1D2-A524 (**d**), D1D2-

277 A483 "closed" conformer (**e**), D1D2-A483 "open" conformer **(g)**. **f**, **h**, higher magnification of the IpaA

278 VBS3-D1D2 interaction in (**e**) and (**g**) showing the distance between residues in Å. IpaA VBS1-3 were

279 docked on the surface of Vinculin D1D2 using MS cross-link constraints. TX-MS protocol in combination

280 with MS constraints was used to unify and adjust the final model, which justifies over 100 cross-links.

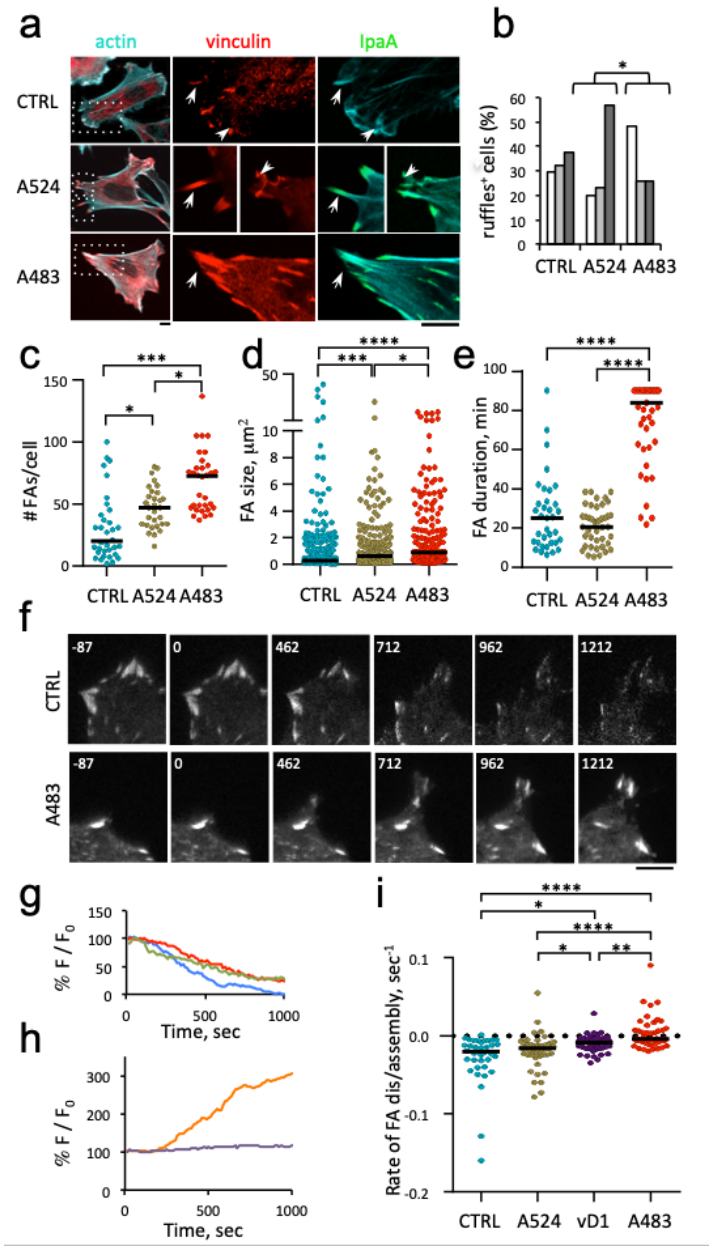

281

282 **Figure 3 – A483 stabilizes vinculin in cell adhesions in the absence of mechanotransduction**

283 **a-c**, Immunofluorescence analysis of vinculin adhesions. CTRL: C2.7 cells. A524: GFP-A524

284 transfectants. A483: GFP-A483 transfectants. **a,** representative fluorescence micrographs. Arrows:

285 adhesions; arrowheads: ruffles. Green: GFP; red: vinculin; cyan: actin. **b**, percent of cells with ruffles ±

286 SEM. Cells with: no ruffles (empty bars); small ruffles (light grey bars); large ruffles (dark grey bars). *:
287 Pearson's Chi-squared test (N=3, n > 30, p = 0.036). **c**, **d**, vinculin containing FAs were detected using a
288 semi-automated program. **c**, median number of FAs per cell; **d**, FA size. (N=3, n > 30). Dunn's multiple
289 comparisons test. *: $p < 0.05$;***: $p < 0.005$. **e**, TIRF microscopy of C2.7 cells transfected with mCherry-
290 vinculin alone (CTRL) or co-transfected with GFP-A524 (A524), GFP-vD1 (vD1), or GFP-A483 (A483). The
291 duration of vinculin-containing adhesions was determined from time-lapse acquisitions. **f-i**, TIRF
292 microscopy analysis of cells treated with 100 μM Y-27632. **f,** Representative time series acquisitions.
293 Numbers indicate the elapsed time in seconds, with the inhibitor added at t = 0. Scale bar = 5 μm. **g, h**,
294 F/F_0: normalized average fluorescence intensity of adhesions as a function of time. Representative traces
295 corresponding to single adhesions for: **h**, control cells: blue, A524: red, vD1: green; **g**, A483: purple and
296 orange. **i,** initial rates of adhesion disassembly inferred from linear fits. N = 5. Number of adhesions
297 analyzed: CTRL: 84; vD1: 75; A524: 140; A483: 97. Dunn's multiple comparisons test. *: $p < 0.05$; **: $p <$
298 0.01;***: $p < 0.005$; ****: $p < 0.001$.

299

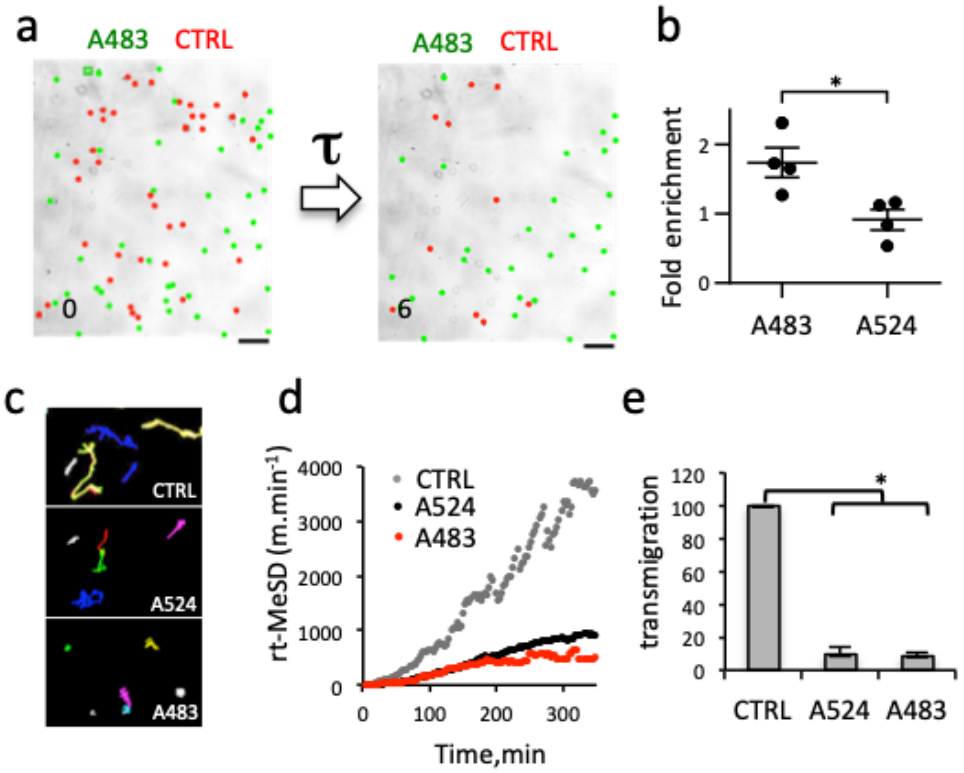

Figure 4. A483-mediated vinculin supra-activation stimulates strong cell adhesion and inhibits tumor cell invasion.

a, b, 1205Lu melanoma cells were transfected with the indicated constructs, labeled with calcein (methods) and mixed with the same ratio of control cells. Cells were perfused in a microfluidic chamber and allowed to adhere for 20 min prior to shear stress application. **a**, representative fields. The number indicates the elapsed time after shear stress application. **b**, Scatterplot of fold enrichment of: A483 (N = 4, n = 610) or A524 (N = 4, n = 433) transfected cells vs control cells (1594 cells, N = 4). Unpaired t test. *: p = 0.0229. **c, d,** cells were transfected with the indicated constructs, and analyzed by time-lapse videomicroscopy. **c**, representative single cell migration 20-hour tracks for indicated samples. **d**, Root of Median Square of displacement over time for control- (61 cells, N = 3), GFP-A524- (61 cells, N = 3) and GFP-A483 transfectants (64 cells, N = 3). ***p = 0.0007. The slopes were analyzed using a covariance test and found to be statistically different (ANCOVA, $p < 2x10^{-16}$). **e,** 5×10^4 cells were seeded in matrigel

314 chambers. The percent of transmigrated cells is indicated. (N = 3). Kruskal-Wallis test with Dunn's

315 multiple comparisons test. *: $p < 0.05$.

316

317

318 **METHODS**

319 **Generation of constructs**

320 Human vinculin constructs were generated by polymerase chain reaction using the forward primer
321 5' GCGCATATGCCAGTGTTTCATACG-3' and reverse primer 5'-CGTCGACTCACCAGGCATCTTCATCGGC-3' for
322 D1 (residues 1-258) or 5'-CGTCGACTCAGTGTACAGCTGCTTTG-3' for D2 (residues 1-492) using a plasmid
323 containing full-length octahistidine-tagged human vinculin (residues 1–1,066), as template[10], and cloned
324 into the NdeI-SalI sites of pet15b (Novagen). The IpaA constructs GFP-A524 and GFP-A483 were
325 generated by polymerase chain reaction (PCR) and cloning into pcDNA3.1 NT-GFP Topo TA (Invitrogen)
326 using the 5'-TCAAAGGACATTACAAAATCC-3' and 5'-GCGATATCATGGCCAGCAAAGG-3' forward primers,
327 respectively, and the 5'-GCGCGGCCGCTTAATCCTTATTGATATTC-3' reverse primer. The GST-A483A
328 construct was generated by PCR using 5'-GGCGAATTCCCGGAGACACATATTTAACACG-3' forward and 5'-
329 GCCGTCGACTTAATCCTTATTGATATTCT-3' reverse primers and cloning into the *EcoRI-SalI* ofpGEX-4T-2
330 (GE Lifesciences). pGST-A524 was previously described[24]. The pGFP-vD1 plasmid was generated by
331 polymerase chain reaction using the forward primer 5'-ACCCGGGATCCCGCC-3' and reverse primer 5'-
332 ACCCGGGACCAGGCA-3', and cloned into peGFP. The pmCherry-human vinculin (HV) and pmCherry-VASP
333 plasmids were from Addgene. Stealth siRNA anti-human vinculin was from Invitrogen (reference number
334 1299001).

335 **Protein purification**

336 BL21 (DE3) chemically competent *E. coli* (Life Technologies) was transformed with the expression
337 constructs. D1 and D1D2 were purified essentially as described[11, 25]. For the IpaA derivatives, bacteria
338 grown until OD_{600nm} = 1.0 were induced with 0.5 mM IPTG and incubated for another 3 hrs. Bacteria
339 were pelleted and washed in binding buffer 25 mM Tris PH 7.4, 100 mM NaCl and 1 mM beta-
340 mercaptoethanol, containing Complete™ protease inhibitor. Bacterial pellets were resuspended in

341 1/50th of the original culture volume and lyzed using a cell disruptor (One shot model, Constant System
342 Inc.). Proteins were purified by affinity chromatography using a GSTrap HP affinity column (GE
343 Healthcare) and size exclusion chromatography (HiLoad S200, Ge Healthcare). Samples were stored
344 aliquoted at -80°C at concentrations ranging from 1 to 10 mg/ml.

345 **Protein complex formation analysis**

346 Proteins were incubated at a concentration of 30 μM in binding buffer for 60 min at 4°C. Samples
347 were analyzed by SEC-MALS (Wyatt Technology Europe) using a 24 ml Superdex 200 Increase 10/300 GL
348 filtration column and a MiniDAWN TREOS equipped with a quasi-elastic light scattering module and a
349 refractometer Optilab T-rEX (Wyatt Technology). Data were analyzed using the ASTRA 6.1.7.17 software
350 (Wyatt Technology Europe). Protein complex formation was visualized by PAGE under non-denaturing
351 conditions using à 7.5% polycrylamide gel, followed by Coomassie blue staining.

352 **Solid-phase binding assay**

353 96–well Maxisorp (Nunc) ELISA plates were coated with 30 nM of full-length vinculin, vinculin
354 constructs or IpaA proteins at the indicated concentrations in binding buffer (25 mM Tris PH 7.4, 100
355 mM NaCl and 1 mM β-mercaptoethanol). Samples were blocked with PBS-BSA 2%, washed and
356 incubated with IpaA or vinculin proteins in binding buffer containing 0.2% BSA at room temperature for
357 one hour. After incubation, the plates were washed and incubated with an anti-IpaA (dilution 1/2000^{e})
358 polyclonal primary antibody[3] or anti-vinculin (dilution 1/2000^{e}) Vin11Vin.5 monoclonal antibody (Sigma-
359 Aldrich) in binding buffer containing 0.2% BSA for one hour at room temperature. Plates were washed
360 and incubated with an HRP-coupled secondary anti-rabbit or anti-mouse IgG antibody (1/32000^{e})
361 (Jackson ImmunoResearch) for one hour. The reaction was revealed by adding 100 μl of
362 tetramethylbenzidine (Sigma-Aldrich) for 15 min, stopped by adding 50 μl of 0.66N H_2SO_4 and the
363 absorbance was read at 450 nm (Dynatech MR400).

364 **BN-PAGE (Blue Native – Polyacrylamide Gel Electrophoresis) protein native gel analysis and**
365 **complex cross-linking**

366 25 μM of vinculin constructs were incubated with different molar ratios of IpaA proteins in a 1X
367 BN-PAGE buffer (250 mM ε-aminicaprionic acid and 25mM Bis-Tris PH 7,0) at 4°C for one hour. The
368 protein mixtures were separated in a one-dimension native BN-PAGE electrophoresis as described[26]. For
369 vinculin-IpaA protein ratio assay, vinculin-IpaA bands containing the complexes separated by BN-PAGE
370 were cut, sliced and boiled in 2 x Laemmli SDS buffer followed by SDS-PAGE. The second dimension SDS-
371 PAGE gels were stained (colloidal Coomassie staining) and the density of the bands was determined
372 using Image J. The normalized vinculin:IpaA ratio of the complexes was compared using a non-
373 parametric Kruskal-Wallis rank sum test (R statistical software).

374 For crosslinking vinculin-IpaA complex, bands containing the complexes were cut, sliced and
375 electroeluted in native conditions (15 mM Bis-Tris pH 7.0 and 50 mM Tricine) inside a closed dialysis
376 membrane (SpectraPor). The soluble complexes were recovered and their buffer exchanged twice into
377 an amine-free cross-link buffer in 25 mM HEPES pH 7.0 containing 100 mM NaCl using 10MWCO ZEBA
378 desalting columns (Thermo Scientific). The fractions containing the complexes were incubated for 1 hr
379 at 4°C with 10 mM N-hydroxysulfosuccinimide and 5 mM EDC (Sigma-Aldrich) following the
380 manufacturer's recommendations. The cross-linking reaction was stopped by adding 50 mM Tris pH 7.4
381 and incubating for 20 minutes. Samples were denaturated in 2x SDS Laemmli buffer for 5 min at 95°C
382 and complexes were eluted from gel slices following SDS-PAGE.

383 **Liquid Chromatography Mass spectrometry (LC-MS)**

384 Complexes obtained after the cross-linking step were loaded onto a 4-20% polyacrylamide gradient gels
385 and Coomassie stained. The bands containing the complexes were cut and submitted to tryptic
386 digestion[27]. The experiments were performed in duplicates for the 3 complexes D1:A524, D1D2:A524
387 and D1D2:A483. Peptides obtained after tryptic digestion were analyzed on a Q Exactive Plus instrument
388 (Thermo Fisher Scientific, Bremen) coupled with an EASY nLC 1 000 chromatography system (Thermo

389 Fisher Scientific, Bremen). Sample was loaded on an in-house packed 50 cm nano-HPLC column (75 µm
390 inner diameter) with C18 resin (1.9 µm particles, 100 Å pore size, Reprosil-Pur Basic C18-HD resin, Dr.
391 Maisch GmbH, Ammerbuch-Entringen, Germany) and equilibrated in 98 % solvent A (H2O, 0.1 % FA) and
392 2 % solvent B (ACN, 0.1 % FA). A 120 minute-gradient of solvent B at 250 nL.min-1 flow rate was applied
393 to separate peptides. The instrument method for the Q Exactive Plus was set up in DDA mode (Data
394 Dependent Acquisition). After a survey scan in the Orbitrap (resolution 70 000), the 10 most intense
395 precursor ions were selected for HCD fragmentation with a normalized collision energy set up to 28.
396 Charge state screening was enabled, and precursors with unknown charge state or a charge state of 1
397 and >7 were excluded. Dynamic exclusion was enabled for 35 or 45 seconds respectively.

398 **Data analysis**

399 The identification of cross-linked peptides from LC-MS data was performed using SIM-XL v. 1.3[28],
400 with the following search parameters: EDC as cross-linker, a tolerance of 20 ppm for precursor and
401 fragment ions, trypsin fully specific digestion with up to three missed cleavages. Carbamidomethylation
402 of cysteines was considered as a fixed modification. All initial identification of cross-linked peptides
403 required a primary score of SIM-XL greater than 2.5 for inter-links and 2.0 for intra-links or loop-links. As
404 single incorrect cross-link identification might lead to a different model, a manual post-validation of the
405 search engine results at the MS2 level was thus performed. A 2D-map showing the protein-protein
406 interaction was generated as an output (Figs. 2a,b). Only peptides present in the 2 replicates are
407 gathered in Supplementary Tables 1-3 and were used for the modeling.

408 **Modeling**

409 We used the constraints obtained from the cross-linking MS data (Suppl. Tables 1-3) to guide the
410 protein structure modeling using the TX-MS protocol as described by Hauri, Khakzad et al.[29]. In short,
411 TX-MS uses the Rosetta comparative modeling protocol (RosettaCM)[30], and the flexible backbone
412 docking protocol (RosettaDock)[31] to generate models and evaluate how well each model explains the MS
413 constraints using a novel scoring function. Here, a total of 100,000 models was generated, of which the

414 highest-scoring model is displayed in (Fig2e), supported by a total of 100 inter and intra-molecular cross-
415 links.

416 **Cell lines**

417 C2.7 myoblasts[32] and MEF vinculin null cells[8] were routinely grown in DMEM 1 g / L glucose
418 containing 10 % FCS in a 37°C incubator containing 10 % CO_2. 1205Lu melanoma cells[33] were grown in
419 RPMI + Glutamax medium (RPMI1640) supplemented with 10 % fetal calf serum (FCS) and non-essential
420 aminoacids in a 37°C incubator with 5 % CO_2.

421 **Immunofluorescence staining**

422 C2.7 mice myoblasts cells were seeded at $2.5x10^4$ cells in 25 mm-diameter coverslips. Cells were
423 transfected with 3 µg of pGFP-A524 or pGFP-A483 plasmids with 6 µl JetPEI transfection reagent
424 (Polyplus) for 16 hours following the manufacturer's recommendations. Cells were fixed in PBS
425 containing 3.7% paraformaldehyde for 20 min at 21°C and permeabilized with 0.1% Triton X-100 for 4
426 min at 21°C. Cells were processed for immunofluorescence staining using the Vin11.5 anti-vinculin
427 monoclonal antibody (ref. V4505, Sigma-Aldrich) and anti-mouse IgG antibody coupled to Alexa 546
428 (Jackson Research) and Phalloidin-Alexa 633 (Invitrogen), as described previously[3]. Samples were
429 analyzed using an Eclipse Ti inverted microscope (Nikon) equipped with a 60 x objective, a CSU-X1
430 spinning disk confocal head (Yokogawa), and a Coolsnap HQ2 camera (Roper Scientific Instruments),
431 controlled by the Metamorph 7.7 software.

432 **TIRF (Total Internal Reflection Microscopy) analysis**

433 C2.7 cells were transfected with pmCherry-HV or pmCherry-VASP and the indicated plasmids as
434 described above. Samples were mounted onto a TIRF microscopy chamber on a stage of an Eclipse Ti
435 inverted microscope (Nikon) equipped with an Apo TIRF 100 x N.A. 1.49 oil objective heated at 37°C. TIRF
436 analysis was performed using the Roper ILAS module and an Evolve EM-CCD camera (Roper Scientific

437 Instruments). When mentioned, Y-27632 was used at 100 µM. Image acquisition was performed every
438 12.5 seconds for 30 to 90 minutes.

439 **Live cell tracking**

440 1205Lu melanoma cells were transfected with IpaA constructs or GFP alone (control) and
441 transferred in microscopy chamber on a 37°C 5%-CO_2 stage in RPMI1640 medium containing 25 mM
442 HEPES. For cell tracking, samples were analyzed using and inverted Leica DRMIBe microscope and a 20 X
443 phase contrast objective. Image acquisitions were performed every 3 min for 200 hrs. The mean velocity
444 of migration was measured for all tracks followed for at least 5 hours. The root square of MdSD over
445 time was plotted over time and fitted by linear regression. The slopes of the linear fit were compared
446 using an ANCOVA test (linear model). The median cell surface was quantified as the mean of the surface
447 for three time points (25%, 50% and 75%) of the whole cell track and dispersion measured by the
448 Median absolute dispersion (MAD).

449 **Invasion assays**

450 Tissue culture Transwell inserts (8 µm pore size; Falcon, Franklin Lakes, NJ) were coated for
451 3 hours with 10 µg of Matrigel following the manufacturer's instructions (Biocoat, BD Biosciences, San
452 Jose, CA). Inserts were placed into 24-well dishes containing 500 µl of RPMI medium supplemented
453 with 1% fetal calf serum. 5×10^4 melanoma cells were added to the upper chamber in 250 µls of serum-
454 free RPMI medium. After 24 hours, transmigrated cells were scored by bright field microscopy.
455 Experiments were performed at least three times, each with duplicate samples.

456 **Image processing and statistical analysis**

457 For the quantification of the number of adhesion structures in C2.7 cells, a semi-automated
458 protocol was developed using Icy software[34]. Spinning-disk fluorescent microscopy planes were used to
459 detect vinculin structures using HK means thresholding and overlaid binary masks obtained from the
460 threshold projections of F-actin labeled images (Max-entropy method). FAs were detected as spots

461 positive for both vinculin mCherry and actin structures using Wavelet Spot Detector. The number of
462 adhesions was analyzed using Dunn's multiple comparisons test. The statistical analysis of cell motility
463 was performed in the R software. Medians were compared using a Wilcoxon rank sum test and
464 dispersion by Median absolute dispersion (MAD) parameter.

465 **Microfluidics cell adhesion assay**

466 Analysis of cell detachment under shear stress was based on previous works[35]. 1205Lu
467 melanocytes were transfected with the indicated constructs, then labeled with 2 µM calcein-AM (Life
468 Technologies) in serum-free DMEM for 20 minutes. Cells were detached by incubation with 2
469 µM Cytochalasin D (Sigma-Aldrich) for 40 minutes to disassemble FAs, followed by incubation in PBS
470 containing 10 mM EDTA for 20 minutes. Cells were washed in EM buffer (120 mM NaCl, 7 mM KCl, 1.8
471 mM $CaCl_2$, 0.8 mM $MgCl_2$, 5 mM glucose and 25 mM HEPES at pH 7.3) by centrifugation and resuspended
472 in the same buffer at a density of 1.5 x 10^6 cells/ml. Calcein-labeled transfected cells and control
473 unlabeled cells were mixed at a 1:1 ratio and perfused onto a 25 mm-diameter glass coverslips
474 (Marienfeld) previously coated with 20 µg/ml fibronectin and blocked with PBS containing 2% BSA
475 (Sigma-Aldrich) in a microfluidic chamber on a microscope stage at 37°C. We used a commercial
476 microfluidic setup (Flow chamber system 1C, Provitro) and a Miniplus3 peristaltic pump (Gilson) to
477 adjust the flow rate in the chamber. Microscopy analysis was performed using a LEICA DMRIBe inverted
478 microscope equipped with a Cascade 512B camera and LED source lights (Roper Instruments), driven by
479 the Metamorph 7.7 software (Universal imaging). Cells were allowed to settle for the indicated time
480 prior to application of a 4 ml/min, flow corresponding to a wall shear stress of 22.2 dyn/cm^2 (2.22 Pa).
481 Acquisition was performed using a 20 X objective using phase contrast and fluorescence illumination
482 (excitation 480 ± 20 nm, emission 527 ± 30 nm). Fluorescent images were acquired before and after
483 flushing to differentiate between target and control cells. Phase contrast images were acquired every
484 200 ms. Fold enrichment was defined as the ratio between of attached labeled and unlabeled cells.

485 **REFERENCES TO METHODS**

486 24 Ramarao, N. *et al.* Capping of actin filaments by vinculin activated by the Shigella IpaA carboxyl-
487 terminal domain. *FEBS letters* **581**, 853-857, doi:10.1016/j.febslet.2007.01.057 (2007).
488 25 Papagrigoriou, E. *et al.* Activation of a vinculin-binding site in the talin rod involves
489 rearrangement of a five-helix bundle. *The EMBO journal* **23**, 2942-2951,
490 doi:10.1038/sj.emboj.7600285 (2004).
491 26 Eubel, H. & Millar, A. H. Systematic monitoring of protein complex composition and abundance
492 by blue-native PAGE. *Cold Spring Harb Protoc*, pdb prot5221, doi:10.1101/pdb.prot5221 (2009).
493 27 Shevchenko A, Tomas H, Havlis J, Olsen JV, Mann M. Nat Protoc. In-gel digestion for mass
494 spectrometric characterization of proteins and proteomes. **1**(6):2856-60 (2006).
495 28 Lima, D. B. et al. SIM-XL: A powerful and user-friendly tool for peptide cross-linking analysis. J
496 Proteomics **129**, 51-55, doi:10.1016/j.jprot.2015.01.013 (2015).
497 29 Hauri, S., Khakzad, H., Happonen, L., Teleman, J., Malmström, J., & Malmström, L. Rapid
498 determination of quaternary protein structures in complex biological samples. Nature
499 communications, **10**(1), 192. doi:10.1038/s41467-018-07986-1 (2019).
500 30 Song, Y. *et al.* High-resolution comparative modeling with RosettaCM. *Structure* **21**, 1735-1742,
501 doi:10.1016/j.str.2013.08.005 (2013).
502 31 Gray, J. J. High-resolution protein-protein docking. *Current opinion in structural biology* **16**, 183-
503 193, doi:10.1016/j.sbi.2006.03.003 (2006).
504 32 Mitrossilis, D. et al. Single-cell response to stiffness exhibits muscle-like behavior. *Proc. Nat.*
505 *Acad. Sci USA.* **106**(43), 18243-18248; https://doi.org/10.1073/pnas.0903994106 (2009).
506 33 Smalley, K. S., et al. Increased cyclin D1 expression can mediate BRAF inhibitor resistance in
507 BRAF V600E-mutated melanomas. *Mol Cancer Ther.,* **7**(9):2876-83. doi: 10.1158/1535-
508 7163.MCT-08-0431 (2008).
509 34 de Chaumont, F. *et al.* Icy: an open bioimage informatics platform for extended reproducible
510 research. *Nat Methods* **9**, 690-696, doi:10.1038/nmeth.2075 (2012).

511 35 Gutierrez, E. *et al.* Microfluidic devices for studies of shear-dependent platelet adhesion. *Lab*

512 *Chip* **8**, 1486-1495, doi:10.1039/b804795b (2008).

513

514

515 **SUPPLEMENTARY INFORMATION**

516

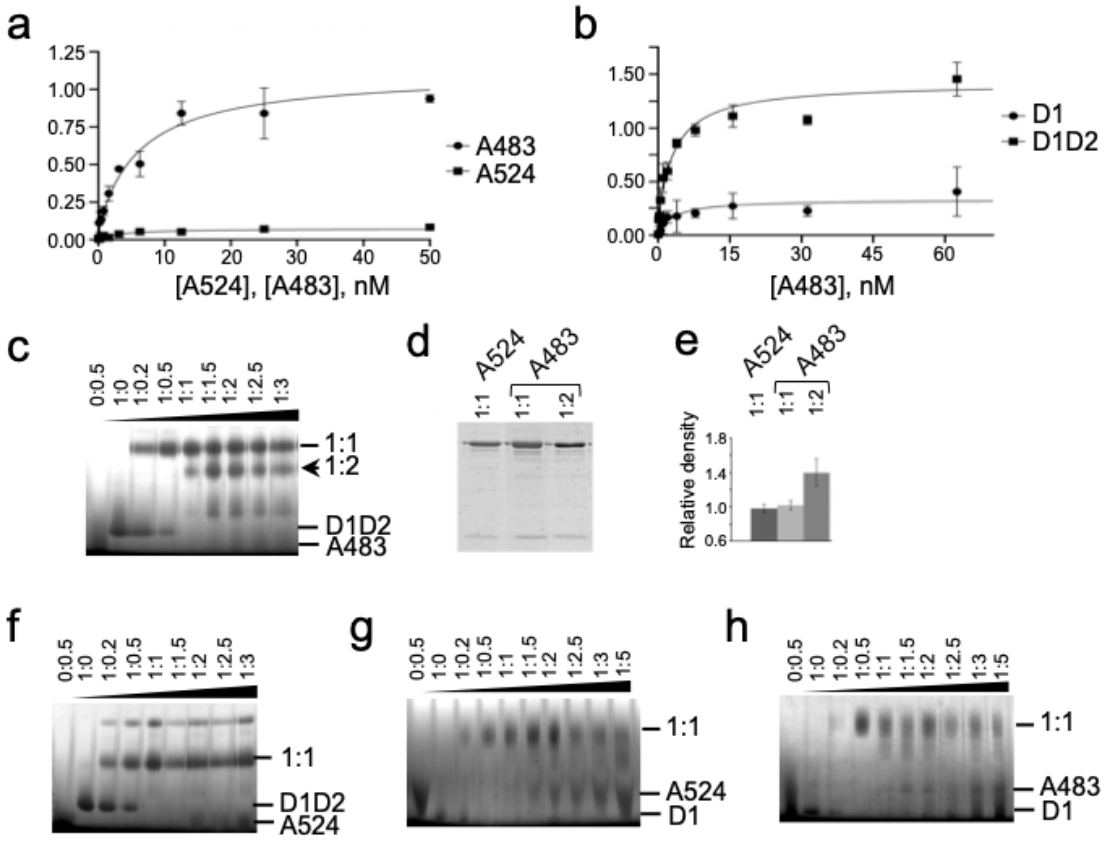

517

518 **Supplementary Fig. 1. IpaA VBS3 reveals multiple binding sites on vinculin.**

519 **a, b,** Solid phase binding assays. **a,** coating: HV; ligands: A483 (solid circles); A524 (solid squares).
520 **b,** coating: D1 (solid circles) or HVD1D2 (solid squares); ligand: A483. **c, f-h,** BN-PAGE in 6-18%
521 polyacrylamide gradient gels and Coomassie staining analysis of D1D2:A483 (**c**), D1D2:A524 (**f**),
522 D1:A524 (**g**) or D1:A483 (**h**) complexes. The molar ratio is indicated above each lane.
523 Arrowheads indicate protein alone, or complex migration at the indicated molar ratio. **d**, bands
524 were recovered from BN-PAGE and analyzed in a second dimension SDS-PAGE in a 15% poly-
525 acrylamide gel and Coomassie staining. Bands were analyzed by densitometry. **e**, ratio of
526 density values for the A524-D1D2 complex (empty bar) and A483-D1D2 complexes
527 corresponding to the upper (light grey bar) or lower (dark grey bar) shifts.

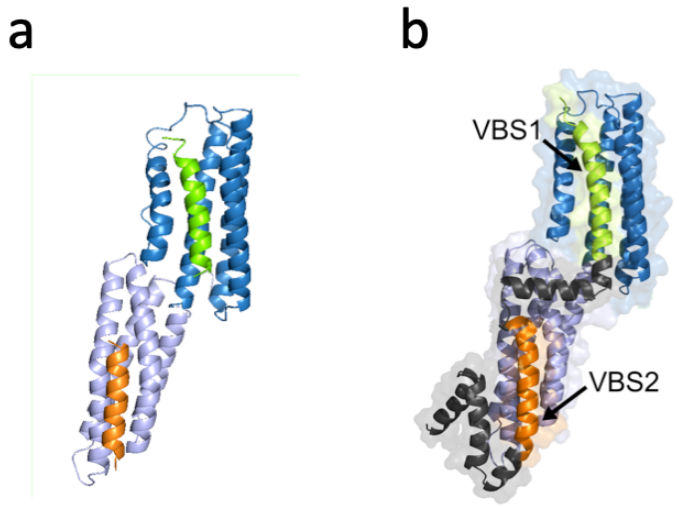

Supplementary Figure 2. Structural models of vD1:A524. a, Structure predicted from the resolved vD1:IpaA VBS1: and vD1:IpaA VBS2 crystal structures[11, 12]**. b,** Structural model of vD1:A524. The model was established using RosettaCM protocol and accounts for 19 inter and intra-molecular cross-links out of 24 identified (Suppl. Table 1).

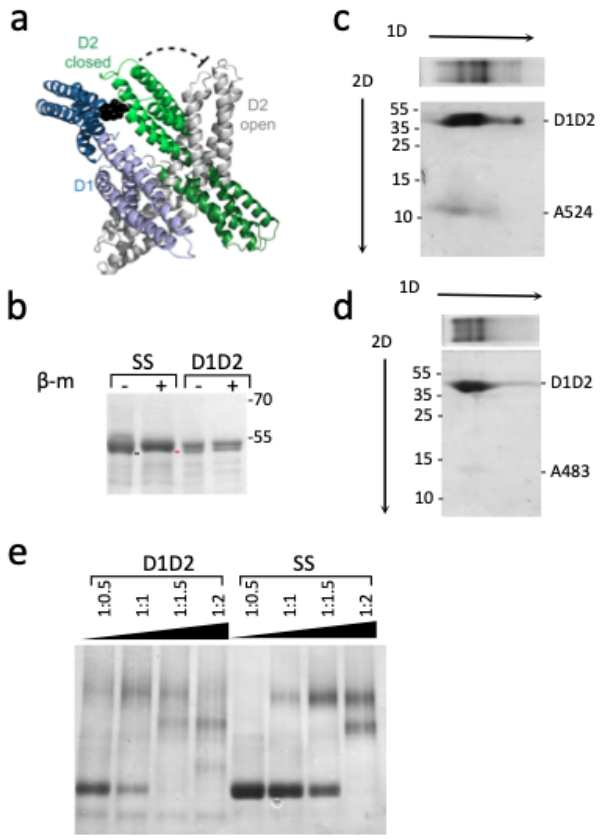

536

537

538 **Supplementary Figure 3. Cysteine-clamped vinculin D1D2 does not form high order complexes.** **a**,
539 Structural model of cystein-clamped vinculin. Blue: D1 domain. Green: D2 domain in the closed
540 conformer. Grey: D2 domain in the open conformer. Black: C68-C396 cystein clamp preventing the
541 switch from closed to open conformers. **b-e**, Coomassie blue staining. **b**, Disulfide bridge formation in
542 D1D2. D1D2: wild-type sequence. SS: D1D2 Q68C A396C. SDS-PAGE analysis using a 10 % polyacrylamide
543 gel. + β-metOH: samples were boiled in Laemmli sample loading buffer containing 5 mM beta-
544 mercaptoethanol prior to SDS-PAGE. The molecular weight markers in kDa are indicated. The black and
545 red bars point the respective migration of unreduced and reduced D1D2 Q68C A396C, respectively. **c**, **d**,
546 gel strips of the native-PAGE corresponding to the A524 + D1D2 (**c**) or A483 + D1D2 (**d**) as shown in **Fig.**
547 **1e** were analyzed in a second dimension by SDS-PAGE using a 10 % polyacrylamide gel as depicted.
548 D1D2, SS, A483 and A524 are indicated. **e**, BN-PAGE analysis in a 6-18% polyacrylamide gradient gel of

549 D1D2:A483 (D1D2) and SS:A483 (SS) complexes. The molar ratio is indicated above each lane.
550 Arrowheads indicate protein alone, or complex migration

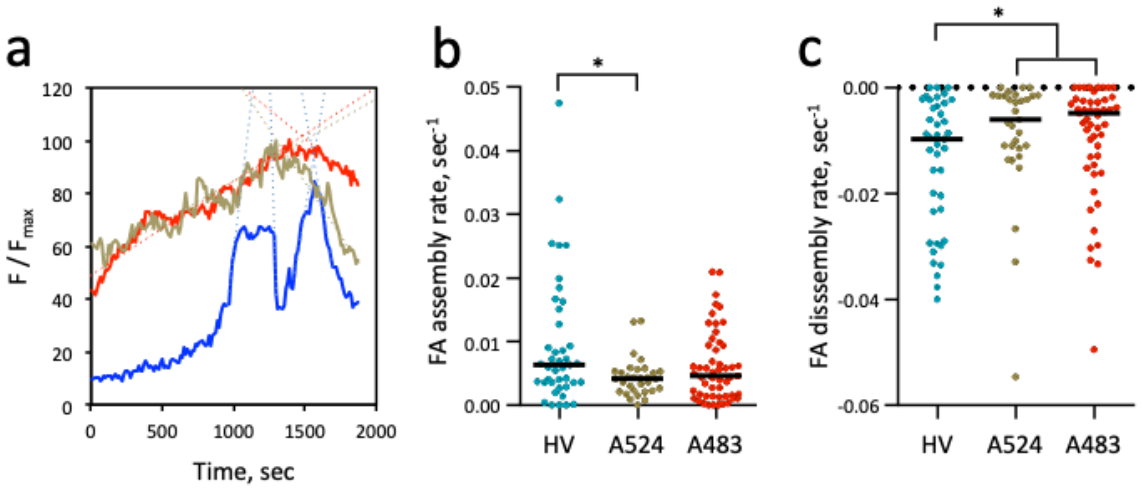

551

552 **Supplementary Figure 4. TIRF analysis of FA dynamics.** C2. 7 cells were transfected with HV-mCherry
553 (HV), HV-mCherry and GFP-A524 (A524) or HV and GFP-A483 (A483). The dynamics of HV-mCherry-
554 labeled FAs were analyzed by TIRF microscopy. **a**, traces correspond to the variations of average
555 fluorescence intensity of a representative single FA (F) normalized to its maximal average fluorescence
556 intensity over the analyzed period in seconds (F_{max}). Blue: HV; green: HV+A524; red: HV+A483. **b**, **c**,
557 instant assembly (**b**) or disassembly (**c**) rates were inferred from the slopes of linear fits as depicted in a),
558 with a Pearson correlation value > 0.85. HV: n = 41, N = 3; HV+A524: n = 31, N = 2; HV+A483: n = 55, N =
559 3. Mann-Whitney U test. *: $p < 0.05$

560

561

562

563

564

565

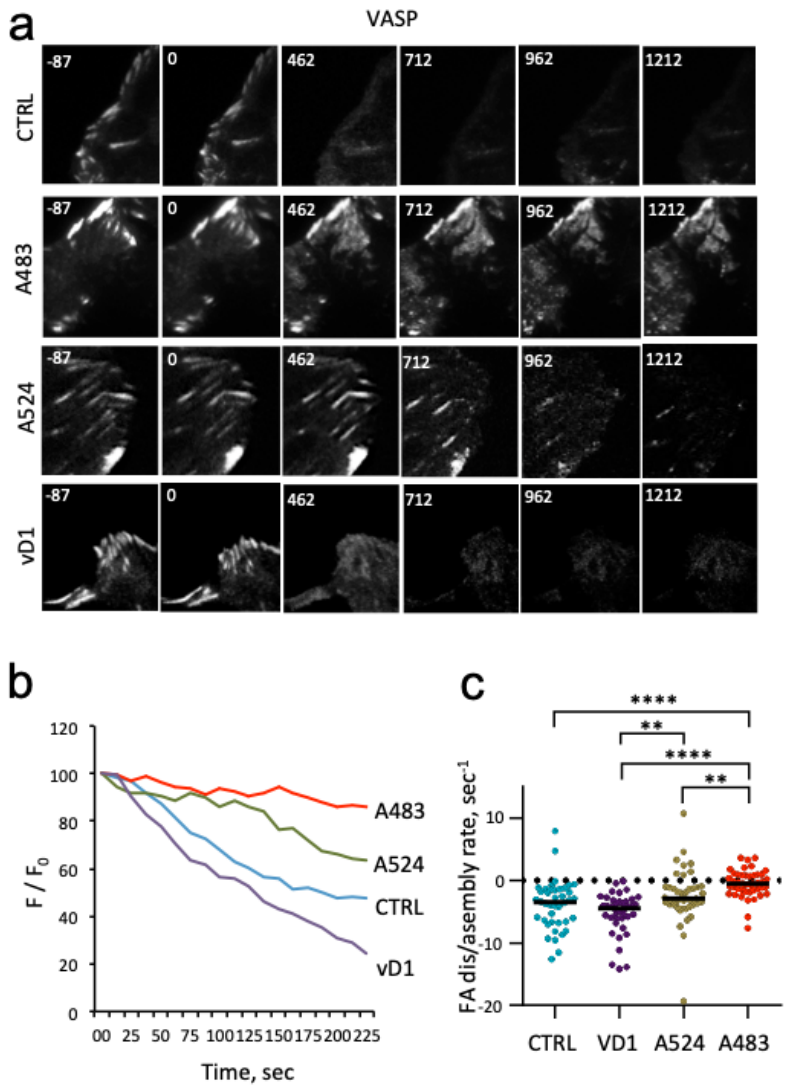

575

576 **Supplementary Figure 5. A483 stabilizes VASP-containing cell adhesions in the absence of**

577 **mechanotransduction**

578 TIRF microscopy of C2.7 cells transfected with mCherry-VASP alone (CTRL) or co-transfected with

579 GFP-A524 (A524), GFP-vD1 (vD1), or GFP-A483 (A483). Adhesion kinetic parameters were determined

580 from time-lapse acquisitions of cells co-transfected with mCherry-VASP and the indicated construct

581 following treatment with 100 µM Y-27632. **a**) Representative time series acquisitions. Numbers indicated

582 the elapsed time in seconds, with the inhibitor added at t = 0. Scale bar = 5 µm. **b**, $\Delta F/F_0$: normalized

583 average fluorescence intensity of adhesions as a function of time. Representative traces corresponding

584 to single adhesions for the indicate samples. **c**, initial rates of adhesion disassembly inferred from linear

585 fits. N = 4. Number of adhesions analyzed: CTRL: 42; A483: 43; A524: 40; vD1: 40. Dunn's multiple

586 comparisons test. *: $p < 0.05$; ****: $p < 0.001$.

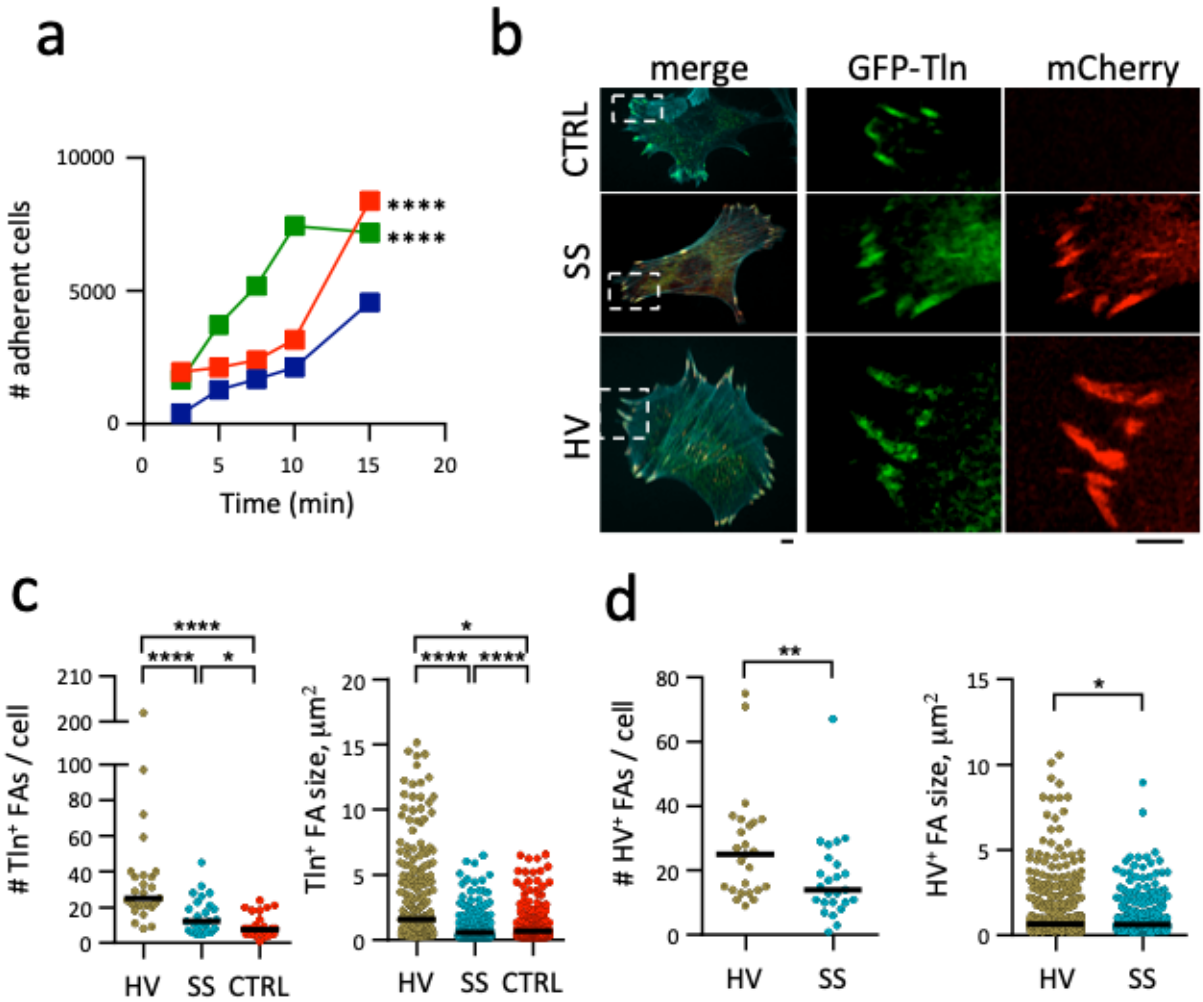

587

588 **Supplementary Figure 6. Effects of A483 and vinculin supra-activation on cell adhesion kinetics**

589 **a**, 1205Lu melanoma cells were transfected with GFP alone (blue), GFP-A524 (red) or GFP-A483 (green), lifted

590 up by trypsinization and plated for the indicated time on Fn-coated coverslips. Samples were washed, fixed and

591 adherent cells were scored microscopically. The total number of adherent cells scored is indicated. GFP: 3223

592 cells, N = 4; GFP-A524: n=7418, N = 4; GFP-A483: n = 5668, N = 4. Chi square corrected with Bonferroni mutliple

593 comparison correction. ****: $p < 0.001$. **b-d**, MEF vinculin null cells were co-transfected with GFP-talin (CTRL)

594 and full length vinculin-mCherry (HV) or HV Q68C A396C-mCherry (SS). Samples were fixed and processed for

595 fluorescence staining of F-actin. **b,** Representative fluorescence micrographs. Red: Vinculin-mCherry; green:

596 GFP-talin; cyan: F-actin. Scale bar = 1 µm. **c**, **d**, FAs were scored using a semi-automatic detection program

597 (Methods) and their number per cell (left) and size (right) are shown. Bar: median size. FAs labeled with: **c**,

598 GFP-talin; **d**, HV or SS. CTRL: n=28, N=3; HV: n = 25 , N = 3; SS: n = 25, N = 3. Mann-Whitney test with

599 Bonferroni multiple comparison correction. * p<0.05; ** p<0.01; *** p<0.005; **** p<0.001.

600

601

602

603

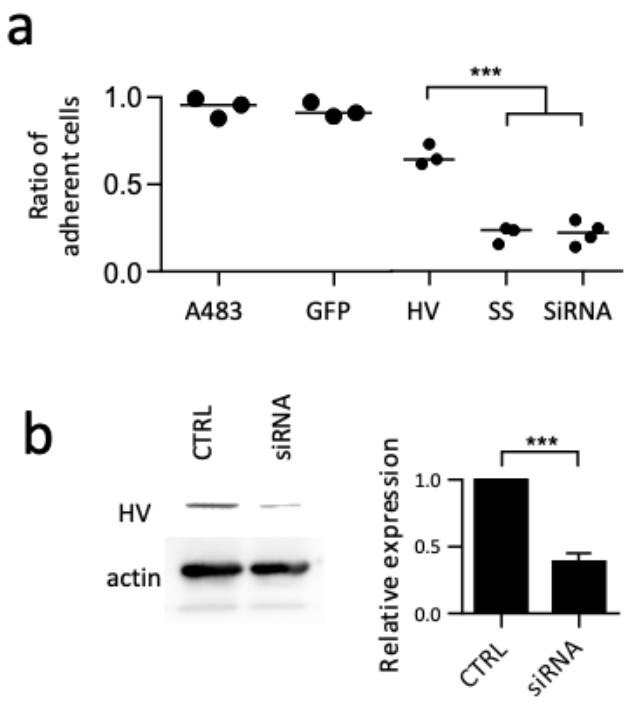

604

605 **Supplementary Figure 7. Role of vinculin supra-activation on cell adhesion.**

606 **a,** 1205Lu melanoma cells were transfected with the indicated constructs, labeled with calcein (methods) and

607 mixed with the same ratio of control cells. Cells were perfused in a microfluidic chamber and allowed to

608 adhere for 30 min (large solid circles) or 15 min (small solid circles) prior to shear stress application. Scatterplot

609 of the ratio of adherent cells: A483 (N = 3, n = 557); GFP (N = 3, n = 490); HV: vinculin mCherry (N = 3, n = 481);

610 SS: vinculin Q68C A396C-mCherry (N = 3, n = 259); siRNA: cells treated with anti-vinculin siRNA (N = 3, n = 395).

611 Unpaired t test. ***: $p < 0.005$. **b**, 1205Lu melanoma cells were mock-transfected (CTRL) or treated with anti-

612 vinculin siRNA (siRNA, Methods). Right: anti-vinculin Western blot analysis. Left: average HV band intensity

613 normalized to that of control cells. Unpaired t test. ***: $p = 0.005$.

614

615 **SUPPLEMENTARY TABLES**

616

#	Exp. MH^+	Primary Score	Peptide Sequence	A524	Hv D1
32670	4457.1	3.28	IDDTSAELLTDDISDLKNNN**D**ITAENNNIYK - MA**K**MIDER	D604	K173
32798	1924.16	2.61	INN**K**LK - **E**LLPVLISAMK	K540	E200
33042	4613.23	3.70	IDDTSAELLT**D**DISDLKNNNDITAENNNIYK - NLGPGMT**K**MAK	D594	K170
33042	4613.23	3.70	IDDTSAELLTD**D**ISDLKNNNDITAENNNIYK - NLGPGMT**K**MAK	D595	K170
33042	4613.23	4.11	IDDTSAELLTDDISDLKNNN**D**ITAENNNIYK - NLGPGMT**K**MAK	D604	K170
33322	5310.64	4.48	IDDTSAELLTDDISDL**K**NNNDITAENNNIYK - VGKETVQTTE**D**QILKR	K600	D67
33334	2347.28	2.51	DVTTSLS**K**VLK - MSA**E**INEIIR	K625	E240
33432	2138.26	2.88	VL**K**NINKD - **E**LLPVLISAMK	K628	E200
33496	2315.32	3.09	AA**K**DVTTSLSK - **E**LLPVLISAMK	K617	E200
34822	2642.55	2.68	AKEVSSALS**K**VLSK - **E**LLPVLISAMK	K579	E200
38218	3685.86	3.87	NIN**K**D - TIESILEPVAQQISHLVIMHEEG**E**VDGK	K632	E31
38218	3685.86	3.66	NIN**K**D - TIESILEPVAQQISHLVIMH**E**EGEVDGK	K632	E28
#	**Exp. MH^+**	**Primary Score**	**Peptide Sequence**	**Hv D1**	
34075	2342.29	3	**E**LLPVLISAMK - NLGPGMT**K**MAK	E200	K170

36135	3088.67	2.62	NFTVE**K**MSAEINEIIR - **E**LLPVLISAMK	K236	E200
#	**Exp. MH$^+$**	**Primary Score**	**Peptide Sequence**	**A524**	
14281	3051.56	3.52	NYVT**E**TNADTIDKNHAIYEK - INN**K**LK	E554	K540
15477	3342.67	2.74	NYVT**E**TNADTIDKNHAIYEK - A**K**EVSSALSK	E554	K571
17603	3141.54	2.71	NYVTETNADTID**K**NHAIYEK - **E**VSSALSK	K562	K572
31359	4483.2	2.64	IDDTSA**E**LLTDDISDLKNNNDITAENNNIYK - A**K**EVSSALSK	E590	K571
31996	2965.5	2.94	IDDTSAELLTDDIS**D**LK - AA**K**DVTTSLSK	D598	K617
31996	2965.5	2.51	IDDTSAELLT**D**DISDLK - AA**K**DVTTSLSK	D594	K617
32705	4586.24	4.1	IDDTSAELLTDDISDLKNNNDITA**E**NNNIYK - AA**K**DVTTSLSK	E608	K617
33253	3291.74	3.81	IDDTSAELLTD**D**ISDLK - AKEVSSALS**K**VLSK	D595	K579
33997	5328.54	4.76	IDDTSAELLTDDISDL**K**NNNDITAENNNIYK - ID**D**TSAELLTDDISDLK	K600	D586
34007	4655.33	4.78	IDDTSAELLT**D**DISDLKNNNDITAENNNIYK - DVTTSLS**K**VLK	D594	K625

Suppl. Table 1. Cross-linked residues characterized in the D1:A524 complex (XL-amino acids of each protein are bolded in the sequences).

#	**Exp. MH$^+$**	**Primary**	**Peptide Sequence**	**A524**	**Hv D1D2**

		Score			
20480	3470.68	3.86	NYVT**E**TNADTIDKNHAIYEK - NLGPGMT**K**MAK	E554	K170
23021	3883.92	3.71	NYVTETNADTID**K**NHAIYEK - **E**TVQTTEDQILKR	K562	E60
24707	3117.73	5.00	AKEVSSALSKVLSK - VGKETVQTT**E**DQILK	K579	E66
36724	4612.22	4.82	IDDTSAELLTDDISDLKNNN**D**ITAENNNIYK - NLGPGMT**K**MAK	D604	K170
39712	5255.49	3.79	IDDTSAELLTDDIS**D**LKNNNDITAENNNIYK - NLGPGMTKMA**K**MIDER	D598	K173
39893	5162.6	4.51	IDDTSA**E**LLTDDISDLKNNNDITAENNNIYK - ALA**K**QVATALQNLQTK	E590	K464
40011	2641.56	4.45	AKEVSSALS**K**VLSK - **E**LLPVLISAMK	K579	E200
41002	3047.64	3.99	L**K**VTDANIR - GILSGTSDLLLTFD**E**AEVR	K542	E128
41440	3944.01	3.86	IDDTSAELLTDDIS**D**LK - AQQVSQGLDVLTA**K**VENAAR	D598	K366
42699	3685.87	4.03	NIN**K**D -TIESILEPVAQQISHLVIMHEEG**E**VDGK	K632	E31
#	**Exp. MH$^+$**	**Primary Score**	**Peptide Sequence**	**Hv D1D2**	
25162	3323.71	4.54	LNQA**K**GWLRDPSASPGDAGEQAIR - ALASI**D**SK	K281	D274
30025	3169.64	4.03	GQGSSPVAMQ**K**AQQVSQGLDVLTAK - V**E**NAAR	K352	E368
30045	3278.66	3.69	VLQLTSWDE**D**AWASK - **K**LEAMTNSKQSIAK	D275	K381
30201	3695.87	3.82	LNQA**K**GWLRDPSASPGDAGEQAIR - MSA**E**INEIIR	K281	E240
31264	3251.77	5.03	ALA**K**QVATALQNLQTKTNR - RQGKGDSP**E**AR	K464	E458
31264	3251.77	4.50	ALA**K**QVATALQNLQTKTNR - RQGKG**D**SPEAR	K464	D455

31620	2516.36	3.44	ALASIDS**K**LNQAK - MSA**E**INEIIR	K295	E240
35256	3787.88	4.12	GILSGTSDLLLTFD**E**AEVR - GSSHHHHHHSS**G**LVPR	E128	G12
38115	3310.75	4.29	GILSGTSDLLLTFD**E**AEVR - AVANSRPA**K**AAVH	E147	K507
39508	3685.90	3.56	GQGSSPVAMQ**K**AQQVSQGLDVLTAK - MSA**E**INEIIR	K352	E240
40134	3129.61	2.19	NQGIEEALKNRNFTVEKMSAEINEIIR	E224	K236
40285	3184.71	4.81	AQQVSQGLDVLTA**K**VENAAR - SLG**E**ISALTSK	K366	E437
40296	2280.32	3.69	**E**LLPVLISAMK - LNQA**K**GWLR	E200	K281
40351	3255.72	4.00	AQQVSQGLDVLTA**K**VENAAR - MSA**E**INEIIR	K366	E240
40571	4536.51	4.44	G**D**SPEARALAKQVATALQNLQTK - SLGEISALTS**K**LADLRRQGK	D455	K444
40881	3704.92	4.32	**K**IDAAQNWLADPNGGPEGEEQIR - **E**LLPVLISAMK	K387	E200
40923	3100.63	3.94	AQQVSQGLDVLTAKV**E**NAAR - **K**LEAMTNSK	E368	K373
41473	3723.01	4.34	GQGSSPVAMQ**K**AQQVSQGLDVLTAK - **E**LLPVLISAMK	K352	E200
41482	4633.41	3.54	TI**E**SILEPVAQQISHLVIMHEEGEVDGK - **K**LEAMTNSKQSIAK	E28	K381
42201	3294.83	3.66	AQQVSQGLDVLTA**K**VENAAR - **E**LLPVLISAMK	K366	E200
#	**Exp. MH$^+$**	**Primary Score**	**Peptide Sequence**	**A524**	
15424	3050.56	3.57	NYVT**E**TNADTIDKNHAIYEK - INN**K**LK	E554	K540
16531	3340.67	3.55	NYVTETNA**D**TIDKNHAIYEK - A**K**EVSSALSK	E558	K571

16865	3341.67	4.11	NYVT**E**TNADTIDKNHAIYEK - A**K**EVSSALSK	E554	K571
34602	4584.25	4.05	IDDTSA**E**LLTDDISDLKNNNDITAENNNIYK - AA**K**DVTTSLSK	E590	K617
35202	4586.25	5.2	IDDTSAELLTDDISDLKNNN**D**ITAENNNIYK - AA**K**DVTTSLSK	D594	K617
35824	4583.26	3.43	IDDTSAELLTDDISDLKNNNDITA**E**NNNIYK - AA**K**DVTTSLSK	E608	K617
39340	4911.48	4.37	IDDTSAELLTD**D**ISDLKNNNDITAENNNIYK - AKEVSSALS**K**VLSK	D595	K579
39340	4911.48	4.06	IDDTSAELLTDDIS**D**LKNNNDITAENNNIYK - AKEVSSALS**K**VLSK	D598	K579
39340	4911.48	3.83	IDDTSA**E**LLTDDISDLKNNNDITAENNNIYK - AKEVSSALS**K**VLSK	E590	K579
39730	3291.74	3.64	IDDTSAELLTD**D**ISDLK - A**K**EVSSALSKVLSK	D595	K571
40244	4655.32	4.35	IDDTSAELLT**D**DISDLKNNNDITAENNNIYK - DVTTSLS**K**VLK	D594	K625
40244	4655.32	4.35	IDDTSAELLTD**D**ISDLKNNNDITAENNNIYK - DVTTSLS**K**VLK	D595	K625

Suppl. Table 2. Cross-linked residues characterized in the D1D2:A524 complex (XL-amino acids of each protein are bolded in the sequences).

632

633

634

635

636

#	Exp. MH^+	Primary Score	Peptide Sequence	A483	Hv D1D2
13237	3014.59	3.29	DIT**K**STTEHR - VGK**E**TVQTTEDQILKR	K530	E66
14671	2518.38	2.49	SKDIT**K** - VGK**E**TVQTTEDQILKR	K526	E66
14791	2556.44	2.35	INN**K**LK - VGK**E**TVQTTEDQILKR	K540	E66
17806	2621.29	3.10	**G**SPGIPGDTYLTR - QQ**E**LTHQEHR	G517	E181
20039	2571.40	3.08	L**K**VTDANIR **-** **E**TVQTTEDQILKR	K542	E66
20526	3651.79	3.37	NYVT**E**TNADTIDKNHAIYEK - NS**K**NQGIEEALK	E554	K219
20985	3469.67	3.01	NYVTETNA**D**TIDKNHAIYEK - NLGPGMT**K**MAK	D558	K170
22936	3468.66	2.62	NYVT**E**TNADTIDKNHAIYEK - NLGPGMT**K**MAK	E554	K170
23137	4011	3.29	NYVTETNADTI**D**KNHAIYEK - VG**K**ETVQTTEDQILK	D561	K59
25418	3725.82	3.27	NYVTETNADTID**K**NHAIYEK - ETVQTT**E**DQILK	K562	E66
25418	3725.82	3.72	NYVTETNADTID**K**NHAIYEK - **E**TVQTTEDQILK	K562	E60
27618	3161.66	3.21	**G**SPGIPGDTYLTR - VGKETVQTT**E**DQILKR	G517	E60
27618	3161.66	3.61	**G**SPGIPGDTYLTR - VGKETVQTTE**D**QILKR	G517	D67
28366	2918.61	3.18	EVSSALS**K**VLSK - VGK**E**TVQTTEDQILK -	K579	E66
29996	1977.96	3.06	**G**SPGIPGDTYLTR - MI**D**ER	G517	D176
36497	2772.45	3.78	**G**SPGIPGDTYLTR - AQQVSQGL**D**VLTAK	G517	D361
36615	4613.23	3.68	IDDTSAELLT**D**DISDLKNNNDITAENNNIYK - NLGPGMT**K**MAK	D594	K170
36632	2214.27	3.22	A**K**EVSSALSK **-** **E**LLPVLISAMK -	K571	E200
37536	3824.86	2.64	**G**SPGIPGDTYLTR - KI**D**AAQNWLADPNGGPEGEEQIR	G517	D389

40263	3413.78	3.79	GSPGIPG**D**TYLTR - AQQVSQGLDVLTA**K**VENAAR	D484	K366
40432	5992.94	5.1	IDDTSA**E**LLTDDISDLKNNNDITAENNNIYK - GQGSSPVAMQKAQQVSQGLDVLTA**K**	E590	K362
40679	2708.42	3.25	S**K**DITK - GILSGTSDLLLTFD**E**AEVR	K526	E128
40994	3074.69	3.12	**K**VTNSLSNLISLIGTK - ETVQTTEDQILK	K498	E66
41187	4612.22	2.86	IDDTSA**E**LLTDDISDLKNNNDITAENNNIYK - NLGPGMT**K**MAK	E590	K170
41816	2387.41	3.65	DVTTSLS**K**VLK - **E**LLPVLISAMK	K625	E200
43326	3137.65	3.41	AAKDVTTSLS**K** - GILSGTSDLLLTFD**E**AEVR	K625	E128
43537	3542.88	3.63	IDDTSAELLT**D**DISDLK - ALA**K**QVATALQNLQTK	D594	K464
43612	3604.91	3.34	VTNSLSNLISLIGT**K**SGTQER - ETVQTT**E**DQILK	K513	E66
45081	3350.71	3.48	**G**SPGIPGDTYLTR - GILSGTS**D**LLLTFDEAEVR	G517	D121
53474	5745.03	4.09	NIN**K**D - TIESILEPVAQQISHLVIMHEEG**E**VDGKAIPDLTAPV AAVQAAVSNLVR	K632	E31
#	**Exp. MH$^+$**	**Primary Score**	**Peptide Sequence**	**Hv D1D2**	
17582	1670.89	3.51	VG**K**ETVQTT**E**DQILK	K59	E66
17582	1670.89	3.38	VG**K**ETVQTTE**D**QILK	K59	D67
26000	3322.71	4.03	LNQA**K**GWLRDPSASPGDAGEQAIR - ALASI**D**SK	K281	D374
30901	3169.64	3.79	GQGSSPVAMQ**K**AQQVSQGLDVLTAK - V**E**NAAR	K352	E368
31031	3695.87	3.81	LNQA**K**GWLRDPSASPGDAGEQAIR - MSA**E**INEIIR	K281	E240
35827	3665.8	3.75	**K**IDAAQNWLADPNGGPEGEEQIR - MSA**E**INEIIR	K387	E240

38215	3040.71	3.43	VG**K**ETVQTTEDQILKR - ELLPVLISAM**K**	K59	K200
39734	3614.9	4.15	GQGSSPVAMQ**K**AQQVSQGLDVLTAK - SLG**E**ISALTSK	K352	E437
40218	3580.72	3.88	VLQLTSWDEDAWAS**K**DTEAMK - MSA**E**INEIIR	K261	E240
40418	2881.63	3.77	QVATALQNLQT**K**TNR - ELLPVLISAM**K**	K476	E200
40559	3184.71	4.71	AQQVSQGLDVLTA**K**VENAAR - SLG**E**ISALTSK	K366	E437
40560	2280.32	3.35	ELLPVLISAM**K** - LNQA**K**GWLR	E200	K281
40604	2553.46	3.78	ALASIDS**K**LNQAK - ELLPVLISAM**K**	K276	E200
41140	2892.69	3.97	ALA**K**QVATALQNLQTK - ELLPVLISAM**K**	K464	E200
41598	4173.16	5.49	GQGSSPVAMQKAQQVSQGLDVLTA**K**VENAAR - KL**E**AMTNSK	K366	E375
41598	4173.16	5.8	GQGSSPVAMQKAQQVSQGLDVLTA**K**VENAAR - **K**LEAMTNSK	E368	K373
41598	4173.16	4.98	GQGSSPVAMQKAQQVSQGL**D**VLTAK - VENAAR**K**LEAMTNSK	D361	K373
41682	3726.02	3.87	GQGSSPVAMQ**K**AQQVSQGLDVLTAK - ELLPVLISAM**K**	K352	E200
42387	3293.83	4.63	AQQVSQGLDVLTA**K**VENAAR - ELLPVLISAM**K**	K366	E200
42387	3293.83	3.3	AQQVSQGLDVLTAKV**E**NAARK - LNQA**K**GWLR	E368	K281
#	**Exp. MH$^+$**	**Primary Score**	**Peptide Sequence**	**A483**	
17398	3339.66	3.31	NYVTETNADTI**D**KNHAIYEK - A**K**EVSSALSK	D561	K571
17630	3341.68	3.44	NYVTETNA**D**TIDKNHAIYEK - A**K**EVSSALSK	D558	K571
17630	3341.68	4.19	NYVT**E**TNADTIDKNHAIYEK - A**K**EVSSALSK	E554	K571

20071	3141.53	3.53	NYVTETNADTID**K**NHAIYEK - AK**E**VSSALSK	K562	E572
20150	3349.69	4.44	NYVTETNA**D**TIDKNHAIYEK - L**K**VTDANIR	D558	K542
20150	3349.69	4.03	NYVTETNADTI**D**KNHAIYEK - L**K**VTDANIR	D561	K542
35163	4584.24	3.59	IDDTSAELLT**D**DISDLKNNNDITAENNNIYK - AA**K**DVTTSLSK	D594	K617
35163	4584.24	3.49	IDDTSAELLTD**D**ISDLKNNNDITAENNNIYK - AA**K**DVTTSLSK	D595	K617
35382	4586.24	3.35	IDDTSA**E**LLTDDISDLKNNNDITAENNNIYK - AA**K**DVTTSLSK	E590	K617
35967	4584.24	4.42	IDDTSAELLTDDIS**D**LKNNNDITAENNNIYK - AA**K**DVTTSLSK	D598	K617
35967	4584.24	4.95	IDDTSAELLTDDISDLKNNNDITA**E**NNNIYK - AA**K**DVTTSLSK	E608	K617
35967	4584.24	4.52	IDDTSAELLTDDISDL**K**NNNDITAENNNIYK - AAK**D**VTTSLSK	K600	D618
35967	4584.24	4.22	IDDTSAELLTDDISDLKNNNDITAENNNIY**K -** AAK**D**VTTSLSK	K614	D618
35967	4584.24	4.94	IDDTSAELLTDDISDLKNNN**D**ITAENNNIYK - AA**K**DVTTSLSK	D604	K617
39881	2845.52	4.73	VTNSLSNLISLIGT**K**SGTQER - **E**LQEK	K513	E520
39881	2845.52	4.62	VTNSLSNLISLIGT**K**SGTQER - ELQ**E**K	K513	E523
40044	4655.33	5.07	IDDTSAELLT**D**DISDLKNNNDITAENNNIYK - DVTTSLSKVL**K**	D594	K625
40044	4655.33	4.86	IDDTSAELLTD**D**ISDLKNNNDITAENNNIYK - DVTTSLSKVL**K**	D595	K625

40044	4655.33	4.45	IDDTSAELLTDDIS**D**LKNNNDITAENNNIYK - DVTTSLSKVL**K**	D598	K625
40044	4655.33	4.44	IDDTSA**E**LLTDDISDLKNNNDITAENNNIYK - DVTTSLSKVL**K**	E590	K625
40065	3092.6	3.51	IDDTSAELLT**D**DISDLK - EVSSALSKVLS**K**	D594	K579
40065	3092.6	3.38	IDDTSAELLTD**D**ISDLK - EVSSALSKVLS**K**	D594	K579
40069	3093.61	3.36	IDDTSAELLTDDIS**D**LK - EVSSALSKVLS**K**	D598	K579
40095	2988.61	4.48	VTNSLSNLISLIGT**K**SGTQER - VT**D**ANIR	K513	D545
40448	3252.74	3.81	VTNSLSNLISLIGT**K**SGTQER - ETIF**E**ASKK	K513	E494
40603	5153.62	4.36	IDDTSAELLT**D**DISDLKNNNDITAENNNIYK - **K**VTNSLSNLISLIGTK	D594	K498
40603	5153.62	4.46	IDDTSAELLTD**D**ISDLKNNNDITAENNNIYK - **K**VTNSLSNLISLIGTK	D595	K498
40603	5153.62	4.56	IDDTSAELLTDDIS**D**LKNNNDITAENNNIYK - **K**VTNSLSNLISLIGTK	D598	K498
40603	5153.62	3.99	IDDTSAELLTDDISDLKNNN**D**ITAENNNIYK - **K**VTNSLSNLISLIGTK	D604	K498
40606	5153.62	3.53	IDDTSA**E**LLTDDISDLKNNNDITAENNNIYK - **K**VTNSLSNLISLIGTK	E590	K498
41116	2593.44	3.85	**K**VTNSLSNLISLIGTK - **E**TIFEASK	K498	E490
41142	3909.09	4	**E**TIFEASKKVTNSLSNLISLIGTK - **G**SPGIPGDTYLTR	E490	G477

Suppl. Table 3. Cross-linked residues characterized in the D1D2 -A483 1:1 complex (XL-amino acids of each protein are bolded in the sequences)

644 **Suppl. movie 1.** TIRF analysis of HV-mCherry expressing C2.7 cells co-transfected with a GFP fusion to
645 the indicated construct. The time is indicated in seconds.
646
647 **Suppl. movie 2.** TIRF analysis of HV-mCherry expressing C2.7 cells co-transfected with a GFP fusion to
648 the indicated construct. The time is indicated in seconds. At time "0", addition of the Rho kinase inhibitor
649 Y-27632 was added at 100 μM final concentration.
650
651 **Suppl. movie3.** TIRF analysis of VASP-mCherry expressing C2.7 cells co-transfected with a GFP fusion to
652 the indicated construct. The time is indicated in seconds. At time "0", addition of the Rho kinase inhibitor
653 Y-27632 was added at 100 μM final concentration.
654
655 **Suppl. Movie 4.** 1205Lu melanoma cells 1205Lu melanoma cells were transfected with the indicated
656 constructs. Cells were perfused in a microfluidic chamber and allowed to adhere for 20 min prior to
657 application of shear stress reaching 22.2 dynes.cm^{-2}. The elapsed time is indicated in seconds.